RF Project 3746
Final Report

the
ohio
state
university

research foundation
1314 kinnear road
columbus, ohio
43212

STUDIES OF HEAT-SOURCE DRIVEN NATURAL CONVECTION: A NUMERICAL INVESTIGATION

A. A. Emara and F. A. Kulacki
Department of Mechanical Engineering

For the Period
July 1, 1975 - June 30, 1977

NATIONAL AERONAUTICS AND SPACE ADMINISTRATION
Theoretical Studies Branch
Ames Research Center
Moffett Field, California 94035

Grant No. NGR-36-008-205

The Ohio State University

August, 1977

STUDIES OF HEAT-SOURCE DRIVEN NATURAL CONVECTION: A NUMERICAL INVESTIGATION

by

A. A. Emara and F. A. Kulacki
Department of Mechanical Engineering
The Ohio State University
Columbus, Ohio 43210

Final Report 3746

Grant NGR-36-008-205

July 1, 1975 - June 30, 1977

NATIONAL AERONAUTICS AND SPACE ADMINISTRATION
Theoretical Studies Branch
Ames Research Center
Moffett Field, California 94035

August, 1977

The Ohio State University Research Foundation
Columbus, Ohio 43212

FOREWORD

The work reported herein was sponsored by the National Aeronautics and Space Administration, Theoretical Studies Branch, Ames Research Center, Moffett Field, California under Grant NGR-36-008-205 and by the Department of Mechanical Engineering. The donation of computer time by The Ohio State University Computer Center and the support of A. A. Emara by the U.S. Nuclear Regulatory Commission under Contract AT-(49-24)-0149 while the present study was under completion is gratefully appreciated. This work was conducted by A. A. Emara under the supervision of F. A. Kulacki in partial fulfillment of the requirements of the Degree of Doctor of Philosophy (in Mechanical Engineering) at The Ohio State University.

ABSTRACT

A numerical study of thermal convection driven by uniform volumetric energy sources has been conducted for a horizontal fluid layer bounded from above by a rigid, isothermal surface and from below by a rigid, zero-heat-flux surface. The side walls of the fluid domain are assumed to be rigid and perfectly insulating. The computations are formally restricted to two-dimensional laminar convection but have been carried out for a range of Rayleigh numbers which spans the regimes of laminar and turbulent flow.

The results of the computations consist of streamline and isotherm patterns, horizontally averaged temperature distributions, and horizontally averaged Nusselt numbers at the upper surface. Flow and temperature fields do not exhibit a steady state, but horizontally averaged Nusselt numbers reach limiting, quasi-steady values for all Rayleigh numbers considered. Correlations of the Nusselt number in terms of the Rayleigh and Prandtl numbers have been determined in the following forms:

$$Nu_1 = 0.477\ Ra^{0.210}\ Pr^{0.0407}$$

$$5 \times 10^3 \leq Ra \leq 5 \times 10^8$$

$$0.05 \leq Pr \leq 20,$$

and

$$Nu_1 = 0.420\ Ra^{0.223}$$

$$5 \times 10^3 \leq Ra \leq 5 \times 10^8$$

$$Pr = 6.5.$$

The latter correlation is in excellent agreement with existing experiments. Horizontally averaged temperature distributions are in good agreement with time-averaged temperature measurements in the layer.

Streamline and isotherm patterns for $Pr = 6.5$ indicate that the convective process is dominated by up-flows of warm fluid over broad regions of the layer. Faster down-flows are confined to narrow regions, and down-flows are always observed on the side walls of the fluid domain. At low Rayleigh numbers, up-flows occur in the center of the layer, and two regions of recirculating flow are observed. At higher Rayleigh numbers, down-flow is observed at the center of the layer with four regions of recirculating flow occupying the layer. For Prandtl numbers other than 6.5, the streamline and isotherm patterns are altered, and the features of these flows are compared with the $Pr = 6.5$ cases for selected Rayleigh numbers.

Blank Page

iv

Page Intentionally Left Blank

TABLE OF CONTENTS

LIST OF FIGURES

LIST OF FIGURES - (Continued)

LIST OF FIGURES - (Continued)

NOMENCLATURE

a	Space- and time-dependent coefficient, Eq. (47)
$a_{i,j}$	Coefficients in Eq. (48)
C	Specific heat
f,F	Function of space and time
g	Constant of gravitational acceleration
H	Volumetric rate of energy generation
h	Convective heat transfer coefficient
i	Location of grid point along x-axis, $i = 1,2,3,\ldots,MM$
j	Location of grid point along y-axis, $j = 1,2,3,\ldots,NN$
$\underline{j}$	Unit vector in y-direction, (0,1,0)
k	Thermal conductivity of fluid
L	Thickness of fluid layer
M	Number of grid lines in x-direction
N	Number of grid lines in y-direction
Nu	Nusselt number, $Nu = \frac{hL}{k}$
p	Pressure
P	Total pressure, Eq. (6)
Pr	Prandtl number, ν/α
Ra	Rayleigh number, $(g\beta/\alpha\nu)\ L^3(HL^2/2k)$
S	Reduced energy source strength, $H/\rho C$
t	Time
Δt	Time increment
T	Temperature
ΔT	Temperature difference across fluid layer

$\underline{u}$	Velocity (u,v)
u	Horizontal component of velocity
v	Vertical component of velocity
X	Horizontal dimension of fluid layer
x	Horizontal Cartesian axis, $0 \leq x \leq X$
Δx	Grid size in x-direction
y	Vertical cartesian axis, $0 \leq y \leq L$
Δy	Grid size in y-direction

Greek Symbols

α	Thermal diffusivity
β	Coefficient of thermal expansion
ϵ	Convergence criterion used in the solution of the stream function-vorticity equation
θ	Temperature deficit, $T-T_r$
ν	Kinematic viscosity
ρ	Density
ψ	Stream function
Ω	Over relaxation factor
ω	Vorticity

Subscripts

c	Critical value for onset of motion
D	Value at down-side to grid point (i,j)
i,j	Grid point location
L	Value at left-side to grid point (i,j)
r	Reference value
R	Value at right-side to grid point (i,j)

U	Value up-side to grid point (i,j)
o	Value at lower surface of fluid layer
1	Value at the upper surface of fluid layer

Superscripts

'	Dimensionless value
*	Referring to time level n + 1
n	Time level

Blank Page

xii - (12)

SECTION I - INTRODUCTION

The purpose of this study is to compute via finite-difference methods the temperature and flow fields of two-dimensional, thermal convection which is driven by uniform volumetric energy sources in a horizontal fluid layer. It is assumed that fluid satisfies the Boussinesq equation of state and is a normal fluid in the sense that $\beta > 0$. The fluid layer is taken to be bounded from above and below by rigid surfaces which are of constant temperature and zero heat flux, respectively. Vertical boundaries of the layer are taken to be perfectly insulating, and the layer aspect ratio (i.e., depth divided by horizontal extent) is varied from 0.125 to 1.0. This variation of the layer aspect ratio is, perhaps, superfluous because the aspect does not appear explicitly in the mathematical formulation of the problem; however, such calculations are performed, in part, as a check on the computational algorithm and for the sake of completeness. Computations are also done for the case of a layer bounded from above and below by two rigid, isothermal surfaces owing to the existence of both experimental [7] and theoretical [12] studies with these boundary conditions.

Additional objectives of the present study are to investigate the influence of the Prandtl number on the flow and temperature fields in the layer and to compute the heat flux at the upper surface of the layer. Owing to both stability and convergence criteria and limitations on computational time, the Prandtl number range considered in the present study is $0.05 \leq Pr \leq 20$. Heat transfer results are presented as correlations in terms of the Nusselt number at the upper surface and the Rayleigh and Prandtl numbers in a form suitable for engineering applications.

From the known theoretical works on thermal convection, it appears that exact solutions for the temperature and flow fields can be obtained only for a relatively small range of Rayleigh numbers via either approximate or exact analytical methods [15]. On the other hand, the application of finite-difference methods to approximate the system of partial differential equations governing the convective process can yield solutions for a larger range of Rayleigh numbers. Numerical work up to the present has treated thermal convection with uniform volumetric energy sources in a horizontal fluid layer, with thermal and hydrodynamic boundary conditions of interest here, only for low Rayleigh number laminar convection, e.g., the numerical work by Thirlby [16] for $1.5 \times 10^3 \leq Ra \leq 2.6 \times 10^4$. Therefore, our goal is to obtain numerical solutions for the flow and temperature fields for Rayleigh numbers larger than those of previous studies.

The computational approach taken in the present study is to cast the governing time-dependent nonlinear partial differential equations in finite-difference form and to seek quasi-steady solutions in terms of a convergence criterion placed on the temperature distribution within the layer. This approach is followed in recognition of studies of Kulacki and Goldstein [7], Mayinger, Jahn, Reineke and Steinberner [12], and

Goldstein, Chu and Kulacki [6] which showed both experimentally and theoretically that in thermal convection with internal energy sources in a layer with two constant temperature boundaries, horizontally averaged two-dimensional temperature and flow fields exhibit no truly steady pattern despite the fact the average heat fluxes at the layer boundaries reach steady values at a given Rayleigh number. It was expected that the same behavior would be found in the present study because the convective and momentum and energy transport processes within the layer are not much affected by the substitution of a zero heat flux surface at the lower boundary.

SECTION II - GOVERNING EQUATIONS

The temperature and flow fields of thermal convection are governed mathematically by a coupled system of nonlinear partial differential equations derived from the conservation requirements for mass, momentum and energy [2]. In these equations, the Boussinesq approximation [13] is used, i.e., all of the thermophysical properties are assumed to be constant except the density in the body force term which is related to temperature by

$$\rho = \rho_r[1 - \beta(T - T_r)] \ , \tag{1}$$

where ρ_r is the density corresponding to the temperature T_r. The conservation equations for mass, momentum, and energy are,

$$\nabla \cdot \underline{u} = 0 \ , \tag{2}$$

$$\frac{\partial \underline{u}}{\partial t} + (\underline{u} \cdot \nabla)\ \underline{u} = -\frac{\nabla p}{\rho} + \underline{g}[1 - \beta(T - T_r)] + \nu\nabla^2\underline{u} \ , \text{ and} \tag{3}$$

$$\frac{\partial T}{\partial t} + (\underline{u} \cdot \nabla)\ T = \alpha\nabla^2 T + \frac{H}{\rho C} \ . \tag{4}$$

By introducing the variables

$$\theta = T - T_r, \ T_r \equiv T_1 \ , \tag{5}$$

$$P = p + \rho g y \ , \text{ and} \tag{6}$$

$$S = H/\rho C \ , \tag{7}$$

the momentum and energy equations become

$$\frac{\partial \underline{u}}{\partial t} + (\underline{u} \cdot \nabla)\ \underline{u} = -\frac{\nabla P}{\rho} + \beta g \theta \underline{j} + \nu\nabla^2\underline{u} \tag{8}$$

and

$$\frac{\partial \theta}{\partial t} + (\underline{u} \cdot \nabla)\ \theta = \alpha\nabla^2\theta + S \ . \tag{9}$$

The conservation equations may be expressed in dimensionless form by introducing the following variables:

$$\left.\begin{aligned} \nabla' &= L\nabla \ , \\ t' &= \frac{t\alpha}{L^2} \ , \\ \underline{u}' &= \frac{\underline{u}}{\alpha/L} \ , \\ P' &= \frac{PL^2}{\rho\nu\alpha} \ , \text{ and} \\ \theta' &= \frac{\theta}{\left(\frac{SL^2}{2\alpha}\right)} \ . \end{aligned}\right\} \tag{10}$$

Equations (2), (8), and (9) can then be written

$$\nabla \cdot \underline{u} = 0 \ , \tag{11}$$

$$\frac{1}{Pr} \cdot \left(\frac{\partial \underline{u}}{\partial t} + (\underline{u} \cdot \nabla)\ \underline{u}\right) = -\nabla P + Ra\ \theta \underline{j} + \nabla^2 \underline{u} \ , \text{ and} \tag{12}$$

$$\frac{\partial \theta}{\partial t} + (\underline{u} \cdot \nabla)\ \theta = \nabla^2 \theta + 2 \ , \tag{13}$$

where the primes have been dropped in Eqs. (11-13).

By taking the curl of the momentum equation, Eq. (12), the pressure term is eliminated under consideration of the identity $\nabla x(\nabla P) = 0$, and Eq. (12) can be written

$$\frac{1}{Pr}\left(\frac{\partial \underline{\omega}}{\partial t} + (\underline{u} \cdot \nabla)\ \underline{\omega}\right) = -Ra\ \frac{\partial \theta}{\partial x}\ \underline{k} + \nabla^2 \underline{\omega} \ , \tag{14}$$

where the vorticity, $\underline{\omega} = \nabla x \underline{u}$, has been introduced.

In the case of two-dimensional processes, the vorticity has only one component and therefore it can be treated as a scalar quantity. Therefore, the energy and momentum equations can be written as

$$\frac{\partial \theta}{\partial t} + \frac{\partial (u\theta)}{\partial x} + \frac{\partial (v\theta)}{\partial y} = \frac{\partial^2 \theta}{\partial x^2} + \frac{\partial^2 \theta}{\partial y^2} + 2 \ , \tag{15}$$

$$\frac{1}{Pr}\left(\frac{\partial \omega}{\partial t} + \frac{\partial (u\omega)}{\partial x} + \frac{\partial (v\omega)}{\partial y}\right) = -Ra\ \frac{\partial \theta}{\partial x} + \frac{\partial^2 \omega}{\partial x^2} + \frac{\partial^2 \omega}{\partial y^2} \ , \tag{16}$$

where the vorticity is defined as

$$\omega = \frac{\partial u}{\partial y} - \frac{\partial v}{\partial x} \ , \tag{17}$$

and the continuity equation, Eq. (11), has been combined with Eqs. (13) and (14).

In order to calculate the velocity field, $\underline{u} = (u,v)$, from the vorticity field, it is useful to introduce the stream function, ψ, which is related to the velocity field by

$$u = \frac{\partial \psi}{\partial y}, \quad v = -\frac{\partial \psi}{\partial x} . \tag{18}$$

From Eqs. (17) and (18), the relation between the vorticity and stream functions can be written as

$$\omega = \frac{\partial^2 \psi}{\partial x^2} + \frac{\partial^2 \psi}{\partial y^2} . \tag{19}$$

Boundary and initial conditions on $\underline{u}$ and θ are next needed to complete the mathematical formulation of the problem posed by Eqs. (15-19). It is assumed that fluid is contained in a rectangular domain whose sides and bottom are insulated and its top is maintained at constant temperature (Fig. 1). Furthermore, all of the boundaries of the domain are assumed to be rigid. Therefore, the thermal and hydrodynamic boundary conditions associated with Eqs. (15-19) can be formulated as the following:

$$x = 0,\ x = X/L \qquad u = v = \psi = 0,\ \partial\theta/\partial x = 0 \tag{20}$$

$$y = 0 \qquad u = v = \psi = 0,\ \partial\theta/\partial y = 0 \tag{21}$$

$$y = 1 \qquad u = v = \psi = 0,\ \theta = 0 \tag{22}$$

The layer is assumed to be at a constant temperature and motionless at $t = 0$. Thus, the initial conditions are

$$\left.\begin{aligned} &u(x,y,0) = v(x,y,0) = 0 , \\ &\psi(x,y,0) = \omega(x,y,0) = 0 , \text{ and} \\ &\theta(x,y,0) = 0 . \end{aligned}\right\} \tag{23}$$

It should be mentioned that additional boundary conditions are needed to obtain the vorticity at the walls. Since the value for the vorticity at the rigid walls is difficult to obtain in an explicit form, an approximate method will be used and this will be discussed in more detail in Section 3.2.

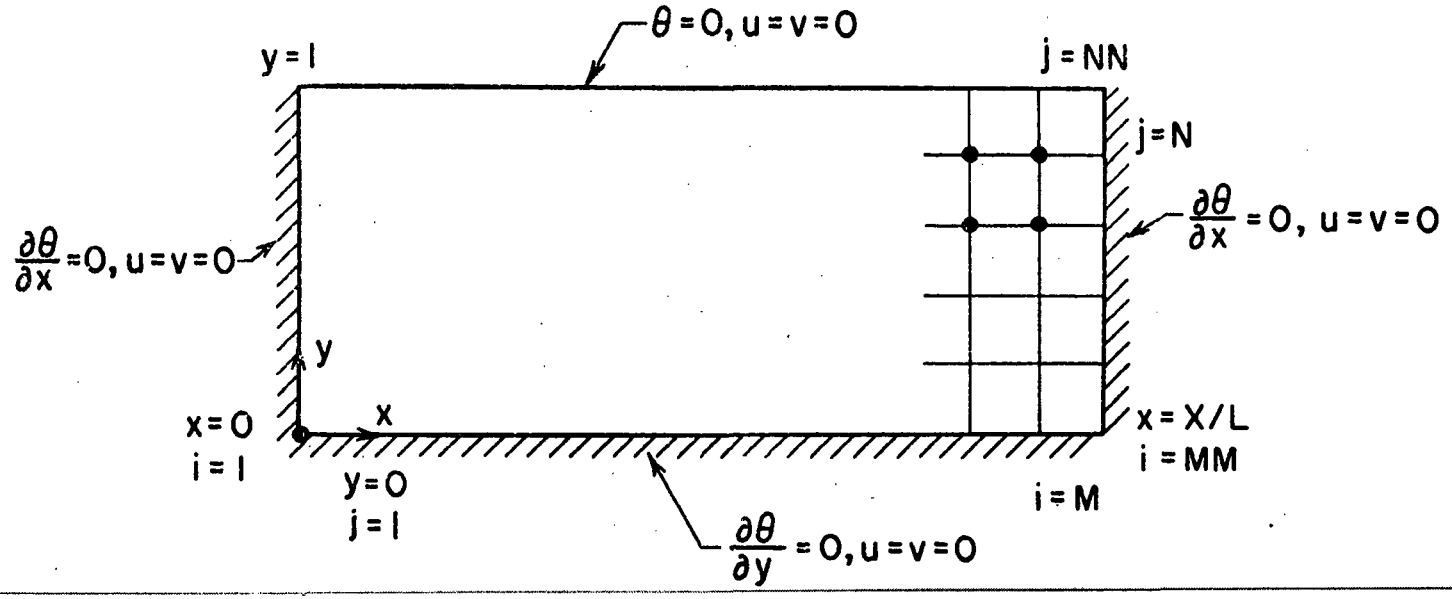

Fig. 1 - Geometry of the layer with coordinate system and thermal and hydrodynamic boundary conditions

SECTION III - THE FINITE-DIFFERENCE SOLUTION

3.1 Formulation of the Finite-Difference Equations

The mathematical description of thermal convection with uniform volumetric energy sources in a horizontal fluid layer by means of coupled, nonlinear partial differential equations makes the exact solution for such a system intractable. Finite-difference methods are of practical value, however, for obtaining an approximate solution to the problem specified by Eqs. (15-23). In order to obtain a solution via finite-differences, the domain of interest is covered with a grid net, and the flow and temperature fields are evaluated only at the grid points at a given point in time. In this study, a grid network is obtained by constructing a series of equally spaced vertical and horizontal lines parallel to the x- and y-axes (Fig. 1). The subscripts i and j are used to denote the positions of the grid points; i.e., $x = (i - 1)\,\Delta x$, $y = (j - 1)\,\Delta y$.

In order to transform Eqs. (15-23) into finite-difference form, a Taylor's series expansion is used to approximate derivatives at a point in terms of the function (e.g., temperature or vorticity) at that point and its neighboring points. Using a Taylor's series expansion for an arbitrary function $f(x,y)$, the following relations can be written:

$$f_{i+1,j} = f_{i,j} + (\Delta x)\left.\frac{\partial f}{\partial x}\right|_{i,j} + \frac{(\Delta x)^2}{2!}\left.\frac{\partial^2 f}{\partial x^2}\right|_{i,j} + \cdots + \frac{(\Delta x)^{m-1}}{(m-1)!}\left.\frac{\partial^{m-1} f}{\partial x^{m-1}}\right|_{i,j} + R_m \,, \tag{24}$$

and

$$f_{i-1,j} = f_{i,j} - (\Delta x)\left.\frac{\partial f}{\partial x}\right|_{i,j} + \frac{(\Delta x)^2}{2!}\left.\frac{\partial^2 f}{\partial x^2}\right|_{i,j} + \cdots + \frac{(-\Delta x)^{m-1}}{(m-1)!}\left.\frac{\partial^{m-1} f}{\partial x^{m-1}}\right|_{i,j} + R_m \,, \tag{25}$$

where R_m is the remainder term. From Eqs. (24) and (25), the following approximations can be written:

$$\left.\frac{\partial f}{\partial x}\right|_{i,j} = \frac{f_{i+1,j} - f_{i,j}}{\Delta x} + O(\Delta x) \,, \tag{26}$$

$$\left.\frac{\partial f}{\partial x}\right|_{i,j} = \frac{f_{i,j} - f_{i-1,j}}{\Delta x} + O(\Delta x) \,, \tag{27}$$

$$\left.\frac{\partial f}{\partial x}\right|_{i,j} = \frac{f_{i+1,j} - f_{i-1,j}}{2\Delta x} + O\left((\Delta x)^2\right) , \text{ and} \tag{28}$$

$$\left.\frac{\partial^2 f}{\partial x^2}\right|_{i,j} = \frac{f_{i+1,j} - 2f_{i,j} + f_{i-1,j}}{(\Delta x)^2} + O\left((\Delta x)^2\right) . \tag{29}$$

Equations (26) and (27) are forward and backward difference approximations, respectively, while Eqs. (28) and (29) are central difference approximations. The last terms in Eqs. (26-29) represent the truncation error and, thus, the accuracy of the finite-difference approximation. It is obvious that the central difference approximations are of higher order accuracy than the other representations. However, from the standpoint of stability requirements, which will be discussed in Section 3.3 below, the representation of the first-order derivatives in Eqs. (15) and (16) by the central difference formulation is useful only for cases where the Rayleigh number is low. In such cases, small grid sizes must be used in order to satisfy the stability requirement. For example, the computations done in this study show that the dimensionless velocities, u and v, reach maximum values on the order of 500 for $Ra = 5 \times 10^6$, which requires Δx and Δy to be less than 0.004. The use of such small grid sizes requires a very large storage capacity in the computer, and moreover, a tremendous amount of computation time. There is, however, no restriction on the grid size when one uses either the backward or the forward difference formulation for the nonlinear terms in Eqs. (15) and (16).

In the early work of Barakat and Clark [1], the nonlinear terms in the energy and vorticity equations were approximated with two-point backward or forward differences according to whether the velocities u and v were either positive or negative, respectively. This was termed the "first upwind differencing method." Torrance [17] developed a modified form of first upwind differencing method in which, for example, the mean x-component of velocity $u = \frac{u_{i,j} + u_{i+1,j}}{2}$, in the nonlinear term $\frac{\partial u\theta}{\partial x}$ of Eq. (15) was multiplied by $\theta_{i,j}$ or $\theta_{i+1,j}$, according to whether u was positive or negative, respectively. The same method was applied to first derivatives with respect to y by replacing the velocity u by v and interchanging i with j. The nonlinear terms in Eq. (16) were similarly treated by replacing θ by ω.

The method developed by Torrance [17], called the "second upwind differencing method"; preserves the conservative and transportive properties of the energy and momentum equations. The second upwind difference formulation of the energy equation, Eq. (15), and the vorticity equation, Eq. (16), both posses the conservative property because the net energy or momentum transport from the boundaries of the grid system into its interior balances the net increase of the energy or momentum within the system [14]. In addition, the second upwind differencing method maintains the transportive property of the governing equations because any perturbation in the velocity, energy, or temperature is advected only in the

direction of the velocity; i.e., downstream with the flow. All methods which use the central difference approximation for the advective terms do not possess this property [14]. Furthermore, Torrance [17] reported that less computation time was needed with the second upwind differencing method than with the first upwind differencing method. Also it was shown by Torrance that the finite-difference representation of the energy and momentum equations using central differences to approximate the advective terms (e.g., in the work of Fromm [5], leads to numerically induced oscillations in the results. Thus, it appears that the use of central differences to approximate the nonlinear terms in Eqs. (15) and (16) can lead to computational difficulties. However, the modified scheme for forward or backward differences developed by Torrance retains some features of central differences, in particular second-order accuracy [14]. Owing to all of these factors, the second upwind differencing method appears to be the most suitable approximation for the nonlinear terms in Eqs. (15) and (16) and has been adopted in the present work.

Finite difference methods for solving parabolic partial differential equations such as the energy and the vorticity equations, Eqs. (15) and (16) respectively, can be classified as either explicit or implicit. The time level at which the spatial derivatives are evaluated determines whether the scheme is explicit or implicit. If the values of the function at the present time, where its values are known at all nodal points, is used in Eqs. (26-29), the scheme is termed explicit. The explicit scheme enables direct computation of the function at all nodal points using a simple marching in time procedure. Use of the explicit method, however, may require small time increments (i.e., large machine time) in order to satisfy stability requirements. To avoid the restriction on the time increment, implicit methods are usually recommended. In the implicit method, iterative techniques are generally used for the solution of the resulting system of algebraic equations. The Gauss-Seidel iteration procedure [19] is suitable for this purpose but may require a large number of iterations per time step. On the other hand, increasing the size of the time step would increase the number of iterations required to achieve any reasonable degree of accuracy. The use of the implicit method from the standpoint of realizing a savings of computation time thus may be of marginal benefit [17]. Furthermore, the use of the implicit method for the solution of the vorticity equation may have a limited advantage over the explicit method owing to the lack of a way to explicitly evaluate vorticity at rigid boundaries. Implicit methods require the use of the vorticity at boundary nodes at time level n + 1 in order to advance the vorticity value at interior nodes from time level n to n + 1. The boundary value of vorticity at time level n + 1 is not known; and therefore, the value of the vorticity at the wall at time level n has to be used to approximate that at time level n + 1. Such a linearization of the vorticity boundary condition requires the use of small time increments so that, ω^n at the boundary will be a good approximation for ω^{n+1}.

With all of the above factors taken into consideration, the explicit formulation of the finite-difference equations has been used in the present study, with the second upwind differencing method developed by

Torrance [17] to approximate the nonlinear terms in Eqs. (15) and (16) and central differences, Eq. (29), to approximate the diffusion terms. The nonlinear spatial derivatives, $\frac{\partial(u\theta)}{\partial x}$, $\frac{\partial(v\theta)}{\partial y}$, $\frac{\partial(u\omega)}{\partial x}$, and $\frac{\partial(v\omega)}{\partial y}$, are approximated with special three-point noncentral differences [14] by

$$\left.\frac{\partial(uf)}{\partial x}\right|_{i,j} = \frac{1}{\Delta x}\left[\left(\frac{u_{i+1,j} + u_{i,j}}{2}\right) f_{i,j} - \left(\frac{u_{i,j} + u_{i-1,j}}{2}\right) f_{i-1,j}\right], \quad (30a)$$

when the terms $\left(u_{i+1,j} + u_{i,j}\right)/2$ and $\left(u_{i,j} + u_{i-1,j}\right)/2$ are both positive, and by

$$\left.\frac{\partial(uf)}{\partial x}\right|_{i,j} = \frac{1}{\Delta x}\left[\left(\frac{u_{i+1,j} + u_{i,j}}{2}\right) f_{i+1,j} - \left(\frac{u_{i,j} + u_{i-1,j}}{2}\right) f_{i,j}\right], \quad (30b)$$

when the terms $\left(u_{i+1,j} + u_{i,j}\right)/2$ and $\left(u_{i,j} + u_{i-1,j}\right)/2$ are both negative. In Eqs. (30a) and (30b), the function f represents either θ or ω. When the average velocities $\left(u_{i+1,j} + u_{i,j}\right)/2$ and $\left(u_{i,j} + u_{i-1,j}\right)/2$ are of different sign, a mixed expression is required which contains one term from each of Eqs. (30a) and (30b), as appropriate. A similar procedure is used to approximate $\frac{\partial(v\theta)}{\partial y}$ and $\frac{\partial(v\omega)}{\partial y}$ according to the sign of $\left(v_{i,j+1} + v_{i,j}\right)/2$ and $\left(v_{i,j} + v_{i,j-1}\right)/2$. The product of the average velocity, for example, $\left(u_{i+1,j} + u_{i,j}\right)/2$ and either $f_{i,j}$ or $f_{i+1,j}$ in Eqs. (30a) and (30b) represents the convective transport of f between node points (i + 1,j) and (i,j). The selection of $f_{i,j}$ or $f_{i+1,j}$, according to the sign of the mean velocity, is necessary for f to be strictly conserved in transport between the nodes.

Equations (15) and (16) can be approximated by the following finite-difference forms:

$$\frac{\theta^*_{i,j} - \theta_{i,j}}{\Delta t} + \frac{\theta_R u_R + \theta_L u_L}{\Delta x} + \frac{\theta_U v_U - \theta_D v_D}{\Delta y}$$

$$= \frac{\theta_{i+1,j} - 2\theta_{i,j} + \theta_{i-1,j}}{(\Delta x)^2} + \frac{\theta_{i,j+1} - 2\theta_{i,j} + \theta_{i-1,j}}{(\Delta y)^2} + 2 , \quad (31)$$

and

$$\frac{\omega^*_{i,j} - \omega_{i,j}}{(\Delta t)} + \frac{\omega_R u_R - \omega_L u_L}{(\Delta x)} + \frac{\omega_U v_U - \omega_D v_D}{(\Delta y)}$$

$$= \mathrm{Pr}\left[\frac{\omega_{i+1,j} - 2\omega_{i,j} + \omega_{i-1,j}}{(\Delta x)^2} + \frac{\omega_{i,j+1} - 2\omega_{i,j} + \omega_{i,j-1}}{(\Delta y)^2}\right]$$

$$- \mathrm{Pr\ Ra}\left[\frac{\theta_{i+1,j} - \theta_{i-1,j}}{2\Delta x}\right], \tag{32}$$

where

$$u_R = (u_{i+1,j} + u_{i,j})/2 , \tag{33}$$

$$u_L = (u_{i,j} + u_{i-1,j})/2 , \tag{34}$$

$$\left.\begin{aligned} f_R &= f_{i,j} \text{ for } u_R > 0 \\ f_R &= f_{i+1,j} \text{ for } u_R < 0 \\ f_L &= f_{i-1,j} \text{ for } u_L > 0 \\ f_L &= f_{i,j} \text{ for } u_L < 0 \end{aligned}\right\}, \tag{35}$$

$$v_U = (v_{i,j+1} + v_{i,j})/2 , \tag{36}$$

$$v_D = (v_{i,j} + v_{i,j-1})/2 , \text{ and} \tag{37}$$

$$\left.\begin{aligned} f_U &= f_{i,j} \text{ for } v_U > 0 \\ f_U &= f_{i,j+1} \text{ for } v_U < 0 \\ f_D &= f_{i,j-1} \text{ for } v_D > 0 \\ f_D &= f_{i,j} \text{ for } v_D < 0 \end{aligned}\right\}. \tag{38}$$

It should be noted that the variable f in Eqs. (35) and (38) represents either θ or ω. The superscript star in Eqs. (31) and (32) denotes the time level n + 1 while all other terms are evaluated at the previous time level n.

By the use of central differences, Eq. (29), to approximate the vorticity-stream function equation, Eq. (19), and the velocities in Eq. (18), one obtains

$$\omega_{i,j} = \frac{\psi_{i+1,j} - 2\psi_{i,j} + \psi_{i-1,j}}{(\Delta x)^2} + \frac{\psi_{i,j+1} - 2\psi_{i,j} + \psi_{i,j-1}}{(\Delta y)^2} , \tag{39}$$

$$u_{i,j} = \frac{\psi_{i,j+1} - \psi_{i,j-1}}{2(\Delta y)} \text{ , and} \tag{40}$$

$$v_{i,j} = -\frac{\psi_{i+1,j} - \psi_{i-1,j}}{2(\Delta x)} \text{ .} \tag{41}$$

3.2 Approximation for the Vorticity at the Boundary

Equation (32) is used to solve for the vorticity at the interior grid points. An explicit relation for the vorticity at rigid boundaries is, however, not possible. Therefore, the following procedure was used to determine approximate values of vorticity on the boundaries.

During a time step, the value of $\omega_{i,j}$ at the boundaries is held constant. After vorticity values at the interior grid points are calculated for the new time step, and the stream function has been computed from it at the same time step using Eq. (39), the values for the vorticity at the boundaries are calculated from the stream function.

The relation for the vorticity at the wall can be derived from a Taylor's series expansion of the stream function and the boundary condition at the rigid wall. For example, at the lower boundary of the layer, $\psi(x,o) = 0$. It follows then that

$$\left.\frac{\partial \psi}{\partial x}\right|_{y=0} = \left.\frac{\partial^2 \psi}{\partial x^2}\right|_{y=0} = 0 \text{ ,}$$

and from Eq. (19), that

$$\omega_{i,1} = \left.\frac{\partial^2 \psi}{\partial y^2}\right|_{y=0} \text{ .} \tag{42}$$

A Taylor's series expansion in y is next used to determine $\psi_{i,2}$ and $\psi_{i,3}$ in terms of $\psi_{i,1}$. Noting that $(\partial\psi/\partial y)_{y=0}$, one obtains

$$8\psi_{i,2} = 4(\Delta y)^2 \left.\frac{\partial^2 \psi}{\partial y^2}\right|_{i,1} + \frac{8(\Delta y)^3}{6} \left.\frac{\partial^3 \psi}{\partial y^3}\right|_{i,1} + O\left((\Delta y)^4\right) \tag{43}$$

and

$$\psi_{i,3} = 2(\Delta y)^2 \left.\frac{\partial^2 \psi}{\partial y^2}\right|_{i,1} + \frac{8(\Delta y)^3}{6} \left.\frac{\partial^3 \psi}{\partial y^3}\right|_{i,1} + O\left((\Delta y)^4\right) \text{ .} \tag{44}$$

From Eqs. (43) and (44), the value of ω at the wall is

$$\omega_{i,1} = \frac{8\psi_{i,2} - \psi_{i,3}}{2(\Delta y)^2} + O\left((\Delta y)^2\right) \text{ .} \tag{45}$$

Similar relations for the vorticity on the other boundaries can also be derived in the same manner. All of the computations done in the present study use Eq. (45) and similar equations to evaluate the vorticity at the boundaries. An exposition of these equations is presented by Emara [4].

It may be noted that Mayinger et al., [12], in their study of thermal convection in an internally heated fluid layer bounded by two constant temperature boundaries, used an expression of first-order accuracy for the vorticity at the walls in the following form:

$$\omega_{i,1} = \frac{2\psi_{i,2}}{(\Delta y)^2} + O(\Delta y) \ . \tag{46}$$

They did not use an expression of second-order accuracy, such as Eq. (45), apparently to avoid numerical instability. It is believed that the source of the numerical instabilities in the work of Mayinger et al. was the use of differencing schemes of different orders of accuracy at the interior grid points and at the boundaries. All of the computations done in the present study to solve for the vorticity at the wall were obtained by using Eq. (45).

In order to determine the possible difference between the results obtained by using Eqs. (45) and (46), a computation was done using Eq. (46). The results of this test computation were in reasonably good agreement with the second-order method. The difference in the heat transfer coefficients at the upper boundary was less than 0.5%.

3.3 The Computational Method

New values of the dependent variables over a time step are computed in the following manner:

1. The calculation is begun by setting the initial conditions $u = v = 0$, $\psi = \omega = 0$, and $\theta = 0$ everywhere in the domain of interest, i.e., $0 \leq y \leq 1$ and $0 \leq x \leq X/L$.

2. The time step, Δt, is determined. This is limited by stability considerations which can be briefly explained by the following: The differential equations of interest can be written in the general form

$$\frac{\partial f}{\partial t} = a_1 \frac{\partial^2 f}{\partial x^2} + a_2 \frac{\partial^2 f}{\partial y^2} + a_3 \frac{\partial f}{\partial x} + a_4 \frac{\partial f}{\partial y} \ , \tag{47}$$

where a_1, a_2, a_3, and a_4 are functions of x, y, and t. An explicit finite-difference method to approximate Eq. (47) reduces it to

$$F^{n+1}_{i,j} = a_{i,j}F^{n}_{i,j} + a_{i+1,j}F^{n}_{i+1,j} + a_{i-1,j}F^{n}_{i-1,j}$$

$$+ a_{i,j+1}F^{n}_{i,j+1} + a_{i,j-1}F^{n}_{i,j-1} \cdot \qquad (48)$$

The coefficients $a_{i,j}\ldots$ denote quantities which are constant over a time step. The quantities $F_{i,j}\ldots$ are functions of x, y, and t and the superscripts n and n + 1 denote time levels t and t + Δt, respectively. Stability in the sense of Lax and Richtmeyer [11] follows if the coefficients $a_{i,j}$ in Eq. (48) are positive, i.e., the equations of the "positive" type if

$$a_{i,j} \geq 0 \qquad (49)$$

for all values of i and j. Another concept defined by Lax and Richtmeyer and usually associated with finite-difference equations is "consistency." A finite-difference equation [e.g., Eq. (48)], is said to be consistent with the given differential equation, Eq. (47), if the truncation error involved in replacing the derivative by finite-differences vanishes as the spatial and time increments both approach zero. Lax and Richtmeyer showed that if the consistency holds, then stability and convergence are equivalent, and moreover stability implies convergence. It is not difficult to show that the present finite-difference formulation of the thermal convection problem can be made to satisfy the stability requirement, Eq. (49). In Eq. (48), all of the coefficients are always positive except $a_{i,j}$, and this coefficient can be made positive by restricting the size of the time step Δt. The resulting finite-difference equations will of the positive type (i.e., stable) provided the following inequality holds when u_R, u_L, v_U, and v_D are positive:

$$\Delta t \leq \left[\frac{u_R}{\Delta x} + \frac{v_U}{\Delta y} + \frac{2}{(\Delta x)^2} + \frac{2}{(\Delta y)^2}\right]^{-1} \qquad (50)$$

for the energy equation, Eq. (31), and

$$\Delta t \leq \left[\frac{u_R}{\Delta x} + \frac{v_U}{\Delta y} + 2\ \mathrm{Pr}\left(\frac{1}{(\Delta x)^2} + \frac{1}{(\Delta y)^2}\right)\right]^{-1} \qquad (51)$$

for the momentum equation, Eq. (32). Similar restrictions on Δt can be derived when u_R, u_L, v_U, and v_D are negative [4].

It may be noted that if the nonlinear terms in the energy equation and the momentum equations are approximated by central differences, then the finite-difference equations are stable when u_R, u_L, v_U, and v_D are positive, provided that

$$\Delta t \leq \left[\frac{2}{(\Delta x)^2} + \frac{2}{(\Delta y)^2}\right]^{-1} \tag{52}$$

and

$$u_R \leq \frac{2}{\Delta x}\ , \quad v_U \leq \frac{2}{\Delta y}\ , \tag{53}$$

for the energy equation, and

$$\Delta t \leq \left[2\ \mathrm{Pr}\left(\frac{1}{(\Delta x)^2} + \frac{1}{(\Delta y)^2}\right)\right]^{-1} \tag{54}$$

and

$$u_R \leq \frac{2\ \mathrm{Pr}}{\Delta x}\ , \quad v_U \leq \frac{2\ \mathrm{Pr}}{\Delta y}\ . \tag{55}$$

for the momentum equation. Similar restrictions on Δt can be derived when u_R, u_L, v_U and v_D are negative [4]. From the inequalities Eq. (53) and Eq. (55), one can see the restrictions on the grid size which is introduced by using central differences to approximate the nonlinear terms in the energy and momentum equations.

3. The temperature distributions at one time step in the future is computed using Eq. (31). The results obtained for the temperature distribution are then used in Eq. (32) to calculate the vorticity at all interior grid points.

4. Equation (39) is then used to find the stream function at all interior grid points. As mentioned earlier, the method of solving the vorticity-stream function equation may be different from that used in solving the energy and vorticity equations. The vorticity-stream function equation is usually solved by an iterative method. The method used in this study is the successive over-relaxation method. The iterative relation for this method as applied to Eq. (39) is

$$\psi'_{i,j} = (1 - \Omega)\,\psi_{i,j} + \frac{\Omega}{\frac{2}{(\Delta x)^2} + \frac{2}{(\Delta y)^2}}\left[\frac{\psi_{i+1,j} + \psi_{i-1,j}}{(\Delta x)^2} + \frac{\psi_{i,j+1} + \psi_{i,j-1}}{(\Delta y)^2} - \omega_{i,j}\right], \tag{56}$$

where Ω is the over-relaxation factor. The iterations are performed on Eq. (56) with an algorithm derived from the Gauss-Seidel [19] iteration method. The convergence criterion observed in computations is

$$\frac{\max\left|\psi_{i,j}^{n+1} - \psi_{i,j}^{n}\right|}{\max\left|\psi_{i,j}^{n+1}\right|} \leq \epsilon \ .$$

For the present study, $\Omega = 1.75$ and $\epsilon = 10^{-4}$.

5. The values of the vorticity at the rigid walls are then calculated using Eq. (45).

6. Finally, Eqs. (40) and (41) are used to compute the velocity components u and v at the interior grid points.

7. Steps 1-7 are repeated until steady state is reached; i.e., the difference between the horizontally averaged temperature distributions of two consecutive time steps is of the order of 10^{-3} over the entire layer.

3.4 The Computation of Heat Flux at the Upper Boundary

The energy flux from the fluid layer to the cooled, isothermal upper boundary was obtained from the temperature field. The local Nusselt number at the upper boundary was defined as

$$Nu_1 = \frac{\partial\theta/\partial y\big|_{y=1}}{\theta_o} \ . \tag{57}$$

The temperature gradient, $\partial\theta/\partial y\big|_{y=1}$, in Eq. (57) was obtained by using a Taylor's series expansion of the temperature, $\theta_{i,j}$, at $j = N$, $j = N - 1$, and $j = N - 2$. When the terms $\partial^2\theta/\partial y^2$ and $\partial^3\theta/\partial y^3$ are eliminated from each of these series expansions, the following expression is obtained for the temperature gradient at the upper boundary:

$$\left.\frac{\partial\theta}{\partial y}\right|_{i,NN} = \frac{18\theta_{i,N} - 9\theta_{i,N-1} + 2\theta_{i,N-2}}{6\Delta y} + \theta\left((\Delta y)^3\right) \ . \tag{58}$$

From the local heat flux developed in this manner, the average value of the Nusselt number was determined by numerical integration using the trapezoidal rule,

$$Nu_1 = \frac{1}{2M}\left[Nu_{1,i=1} + Nu_{1,i=MM} + 2\sum_{i=2}^{M} Nu_{1,i}\right] \ . \tag{59}$$

SECTION IV - PRESENTATION AND DISCUSSION OF RESULTS

4.1 Comparison with Previous Studies

A comparison with the numerical work of Mayinger et al. [12] and the experimental work of Kulacki and Goldstein [7] was run in order to test the precision of the numerical scheme used in the present study. The work of Mayinger et al. and Kulacki and Goldstein treated thermal convection in an internally heated fluid layer confined between two constant-temperature, rigid plates. In Fig. 2, isotherms and streamlines calculated by the method of this study are compared with isotherms and streamlines obtained by Mayinger et al. In Figs. 3-5, the average temperature distributions obtained from the numerical scheme of this work are compared to the spatially averaged temperature distributions obtained experimentally by Kulacki and Goldstein. In both cases, the agreement is good. In Fig. 6, Nusselt number versus Rayleigh number correlations obtained with the numerical method of this study and the correlations of Mayinger et al. and Kulacki and Goldstein are presented. The agreement between the three correlations is seen to be very good, and the numerically derived correlations of the present study lie within the scatter of the data in the experimental correlation of Kulacki and Goldstein.

4.2 Results of the Present Study

Flow fields, temperature fields, and average heat transfer coefficients at the upper surface were obtained for $5 \times 10^3 \leq Ra \leq 5 \times 10^8$, $0.05 \leq Pr \leq 20$, and $0.125 \leq L/X \leq 1$ in the present study. The majority of the computations were done with layer aspect ratios of 1.0 and 0.5. The results presented in this section are for steady convection in accordance with the criterion for steady state solutions described in Section 3.3. All of the results were obtained using a grid size of $\Delta x = \Delta y = 0.033$, which was chosen based on a consideration of accuracy and computation time [4].

In Figs. 7-20, typical streamline and isotherm patterns are presented for $Pr = 6.5$ and several values of Rayleigh number. The results for each value of Ra are presented at the same dimensionless time from the initiation of the computation to facilitate comparison. It should be noted that the results presented in Figs. 7-20 are not truly steady. This characteristic unsteadiness of thermal convection in fluid layers with uniform volumetric energy sources has been observed in experiments [7,12] and also in the present and previous theoretical studies [12].

At a Rayleigh number of 5×10^4 ($Ra/Ra_c = 36$ where $Ra = 1386$ [10]), it is seen in Fig. 7 that two counter-rotating swirls (i.e., vortex-like flows) occupy the fluid layer. This flow acts to carry warm fluid upward over a relatively broad region in the center of the layer (Fig. 8). Cool fluid is carried across the upper boundary and down the side walls of the layer. It may be noted that the cool down-flows and the warm up-flow

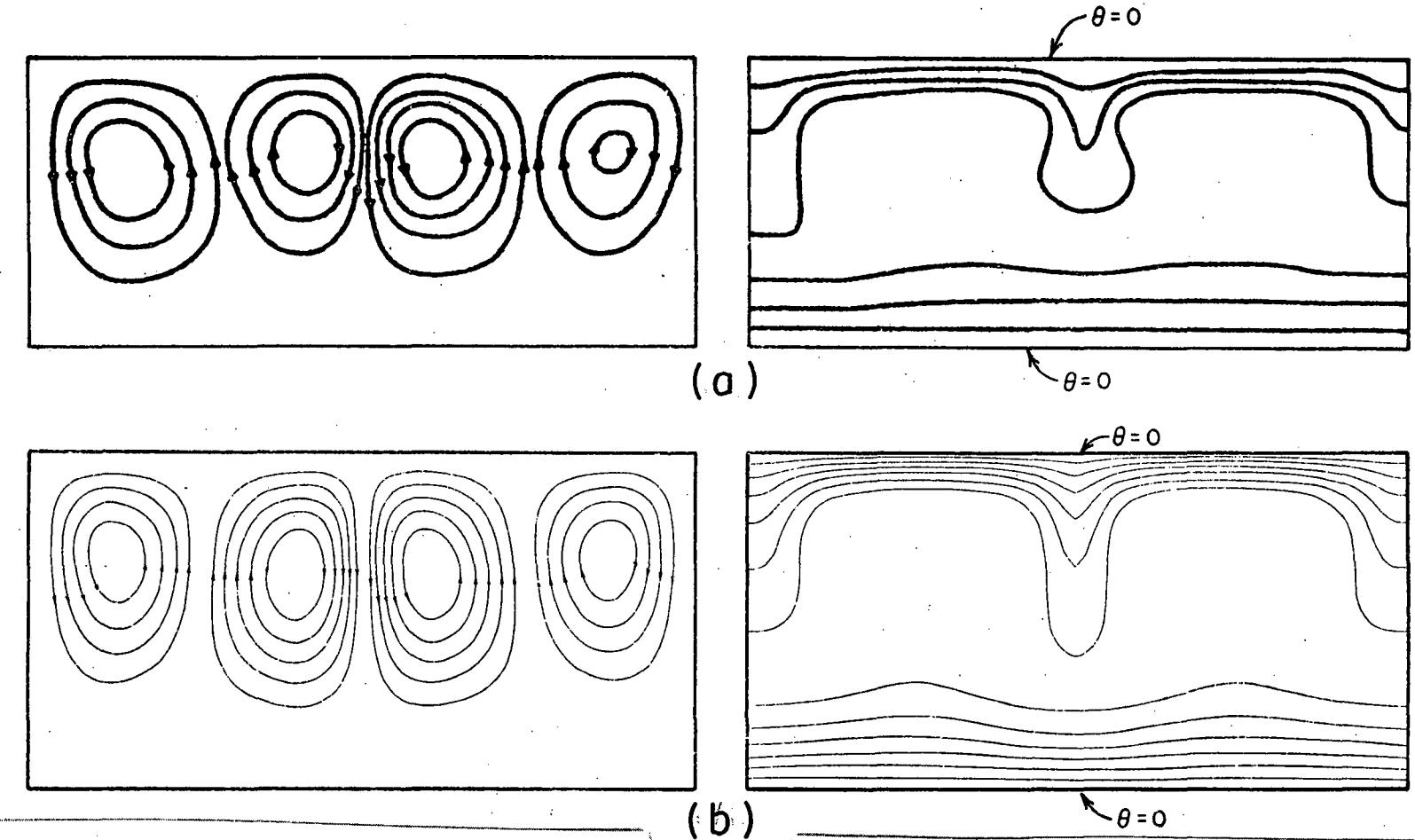

Fig. 2 - Isotherms and streamlines for a layer bounded by two rigid, constant temperature boundaries. Ra = 6.3 x 10^5. (a) Mayinger *et al.* [12]. (b) The present study

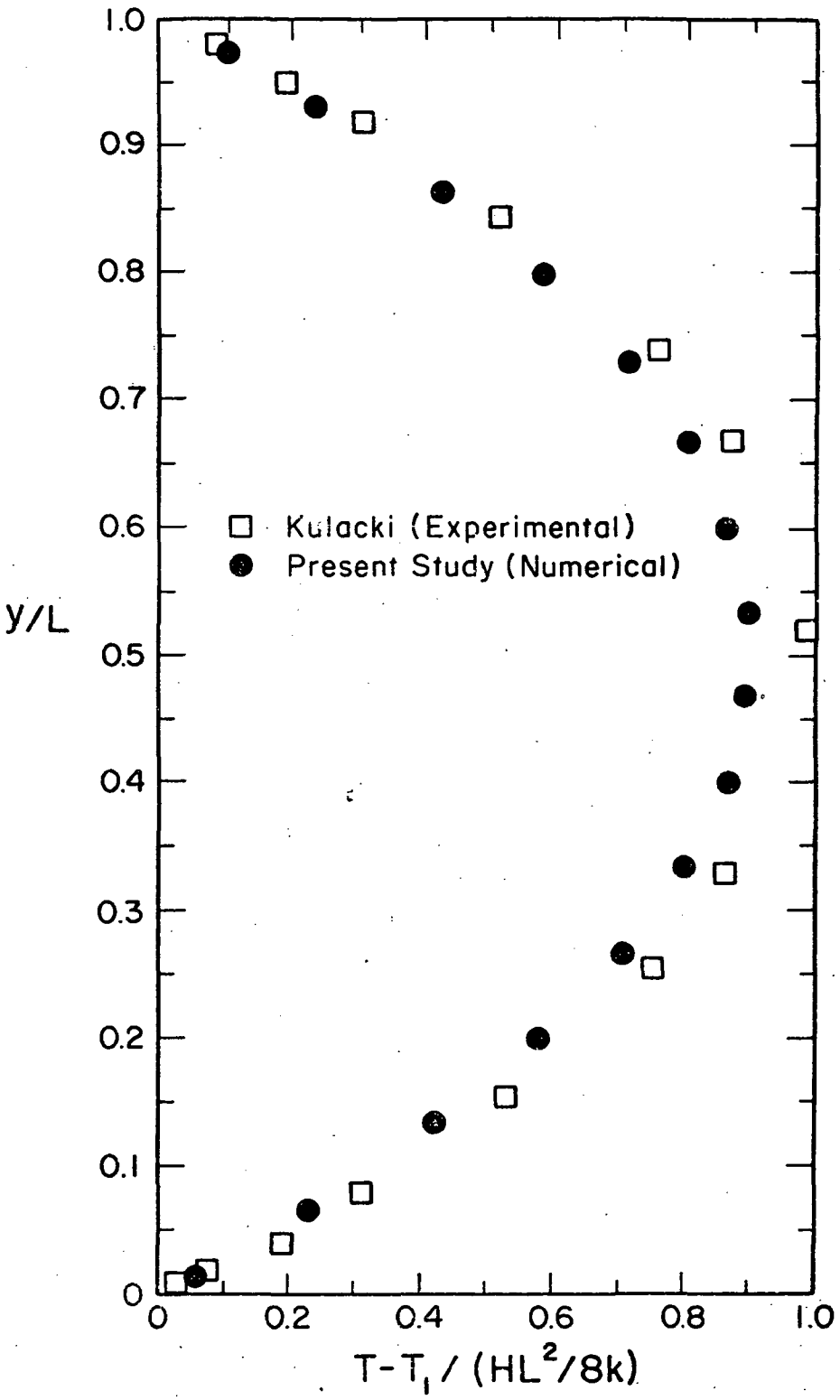

Fig. 3 - Horizontally averaged temperature distribution of Kulacki and Goldstein [7] and the present study for a layer with two rigid isothermal horizontal boundaries. Ra = 5.13×10^4

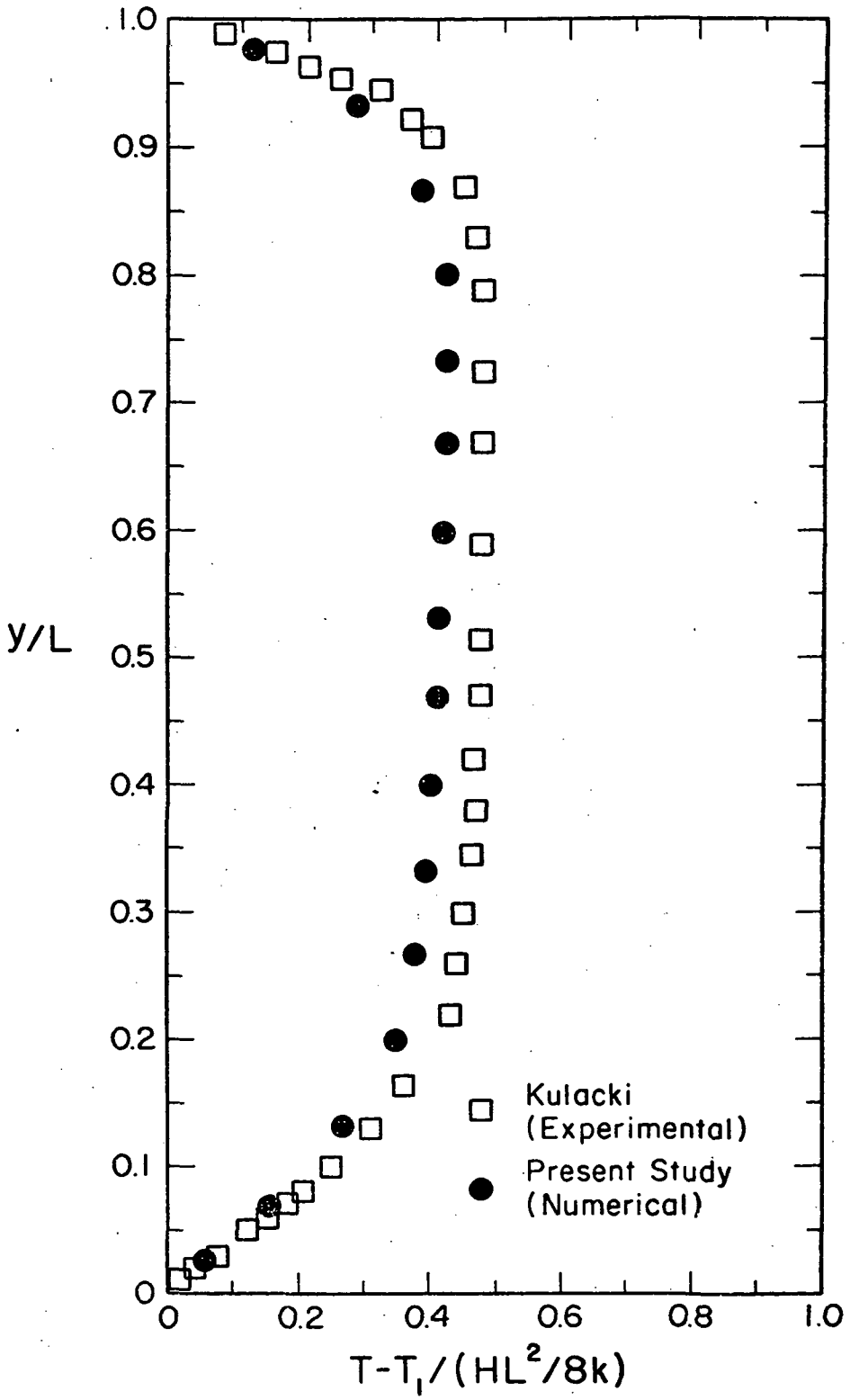

Fig. 4 - Horizontally averaged temperature distribution of Kulacki and Goldstein [7] and the present study for a layer with two rigid isothermal horizontal boundaries. Ra = 4.04×10^6

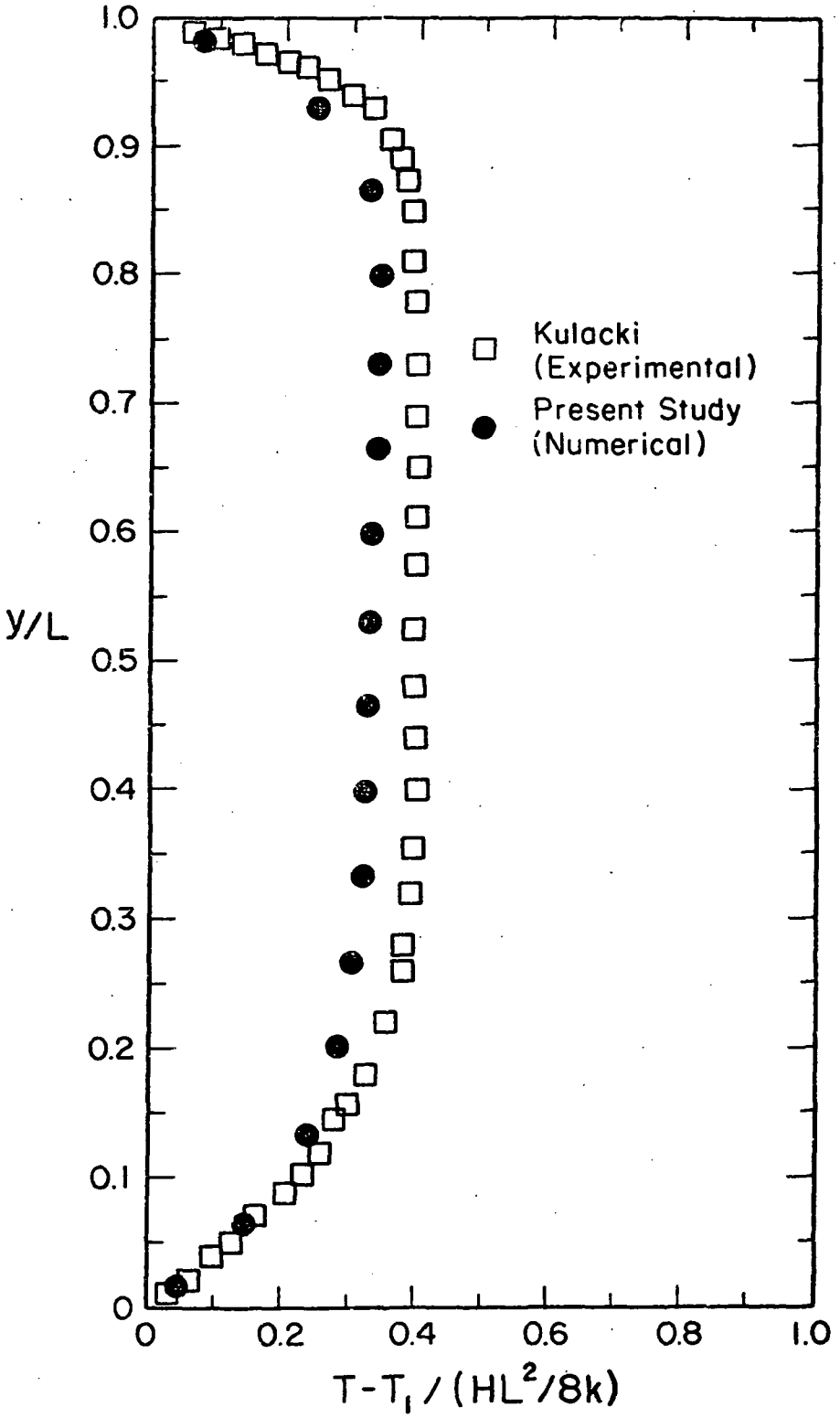

Fig. 5 - Horizontally averaged temperature distribution of Kulacki and Goldstein [7] and the present study for a layer with two rigid isothermal horizontal boundaries. Ra = 1.29×10^7

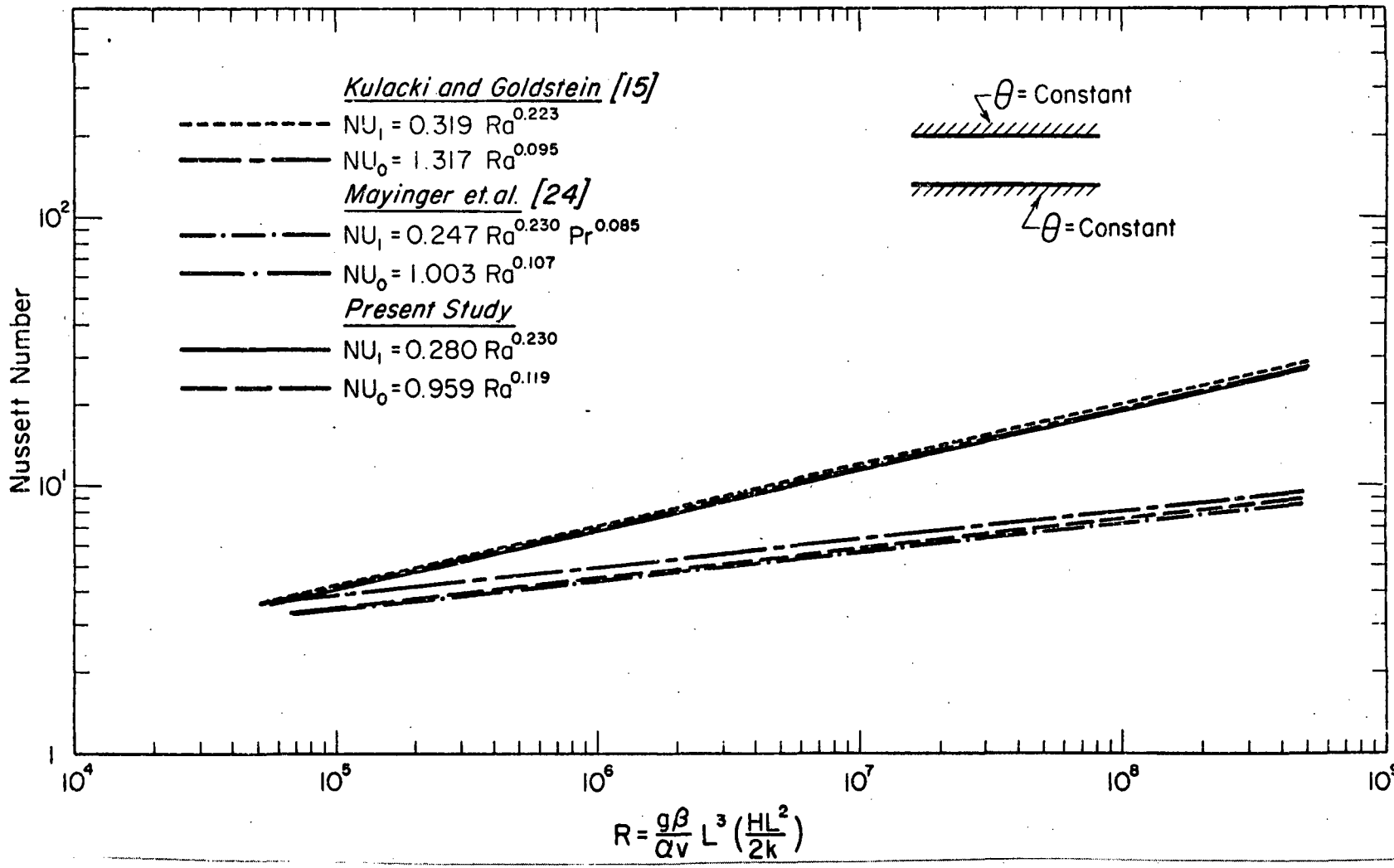

Fig. 6 - Heat transfer correlations of Kulacki and Goldstein [7], Mayinger et al. [12], and the present study for a layer with two isothermal horizontal boundaries

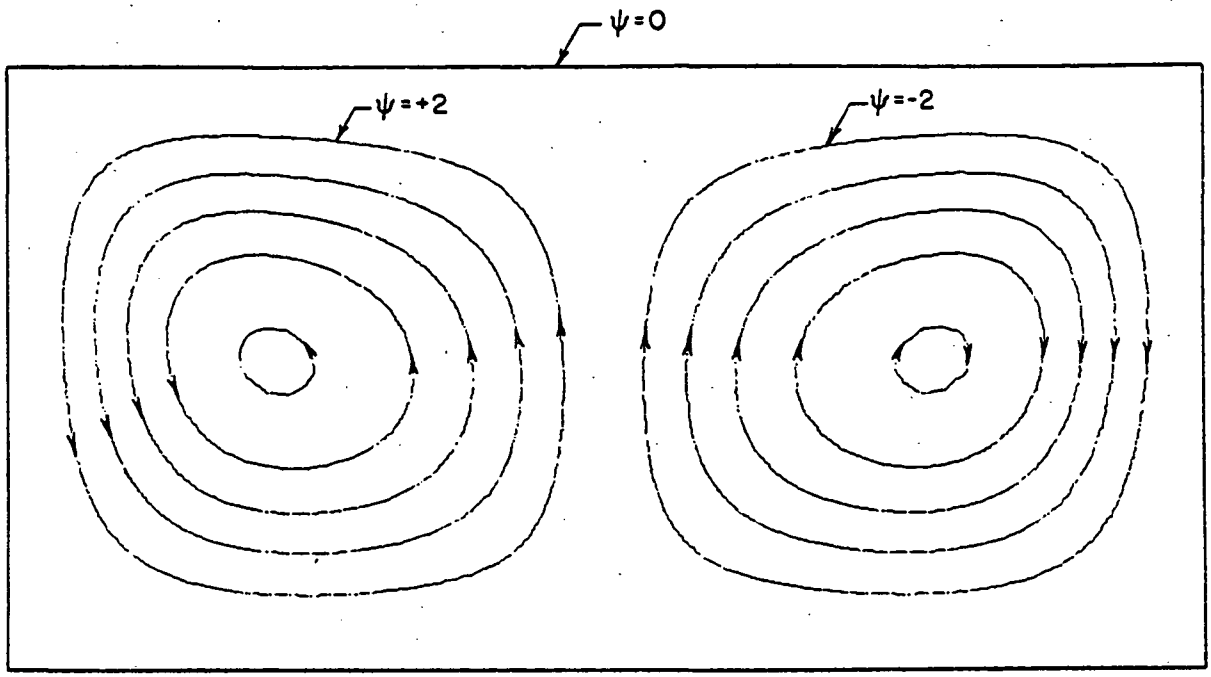

Fig. 7 - Streamline pattern. Ra = 5 x 10^4 and Pr = 6.5

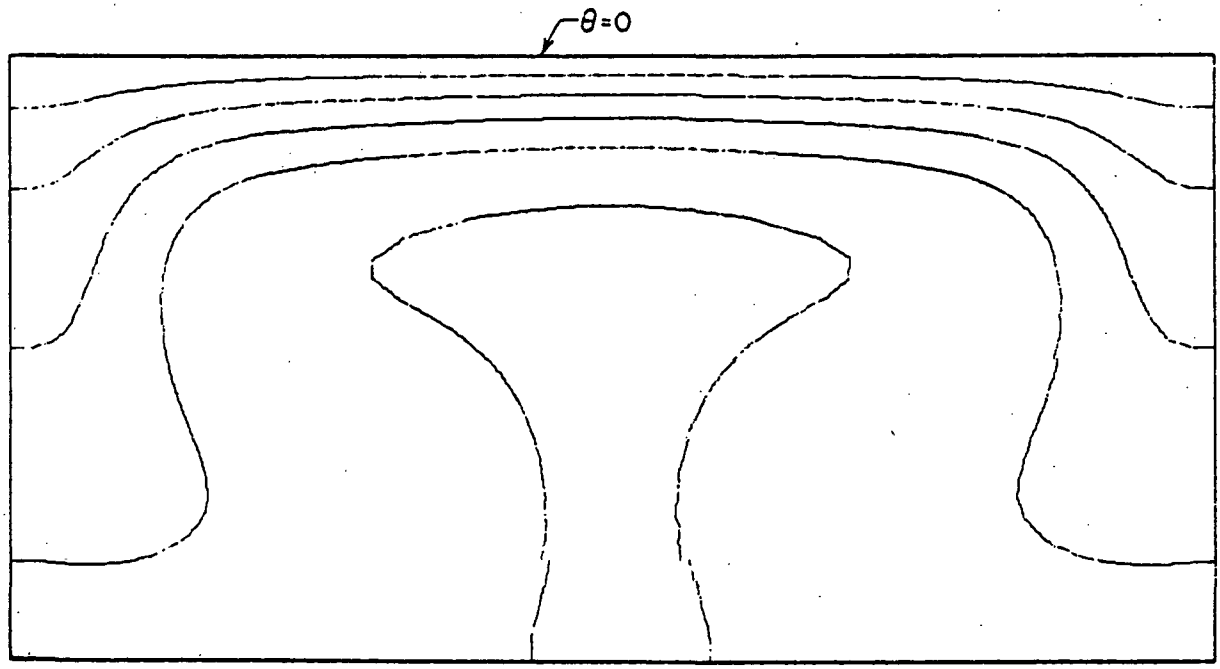

Fig. 8 - Isotherm pattern. Ra = 5 x 10^4, Pr = 6.5, and $\Delta\theta$ = 0.065

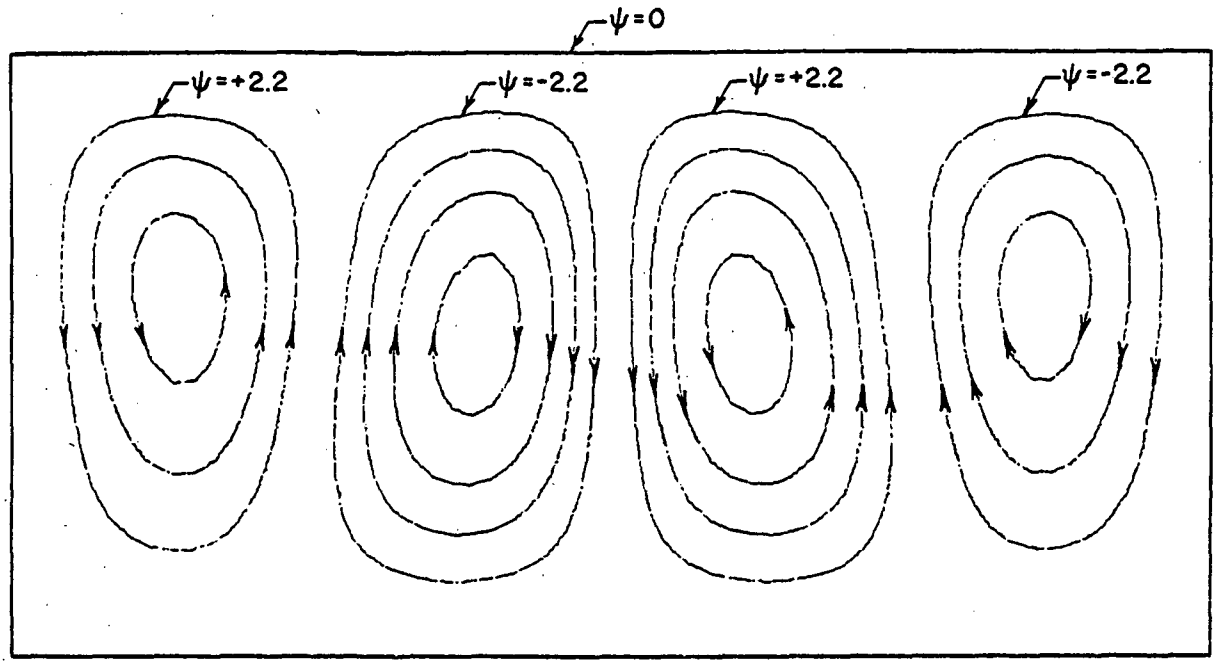

Fig. 9 - Streamline pattern. Ra = 10^5 and Pr = 6.5

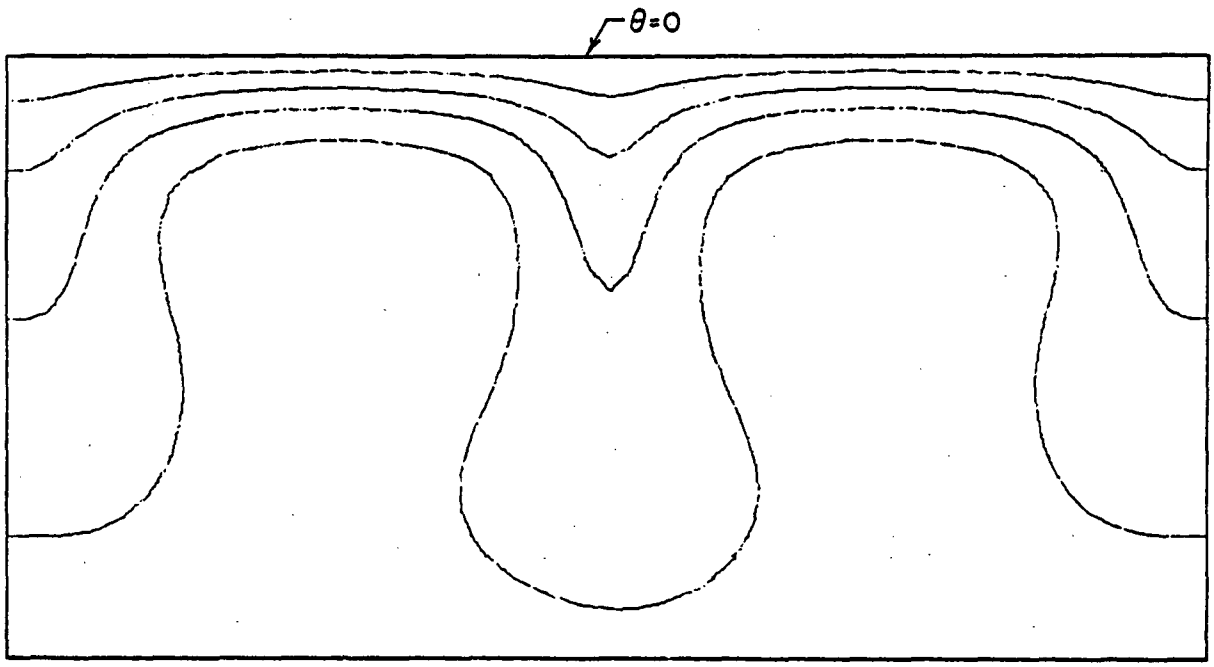

Fig. 10 - Isotherm pattern. Ra = 10^5, Pr = 6.5, and $\Delta\theta$ = 0.06

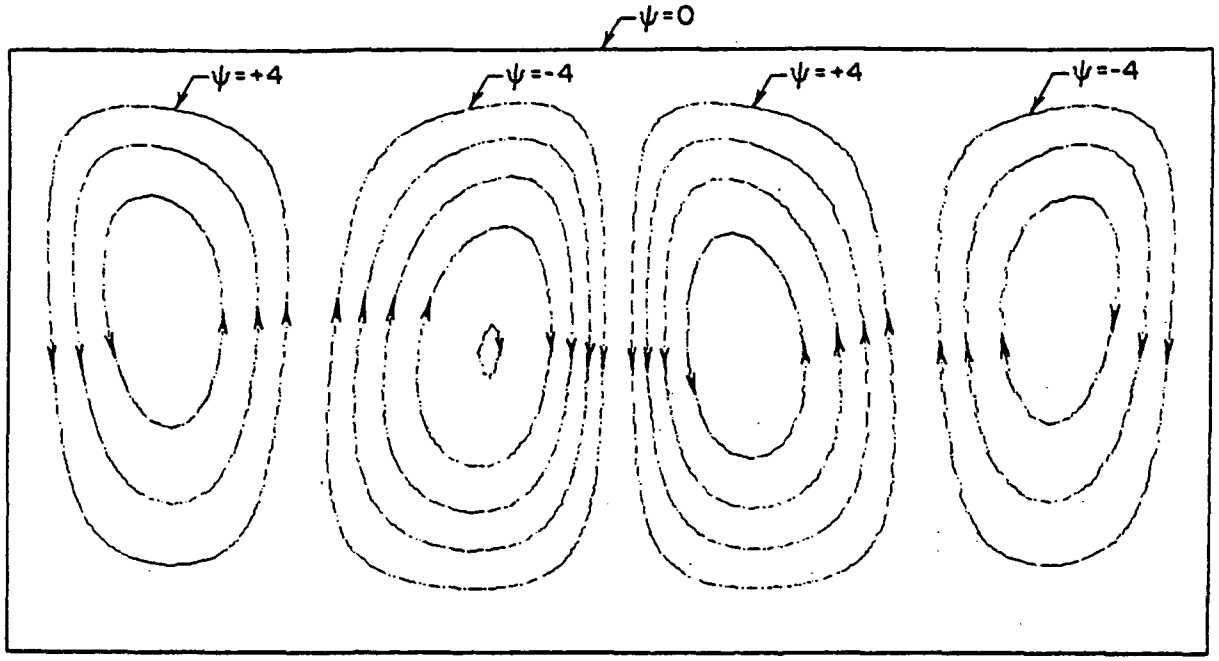

Fig. 11 - Streamline pattern. Ra = 5 x 10^5 and Pr = 6.5

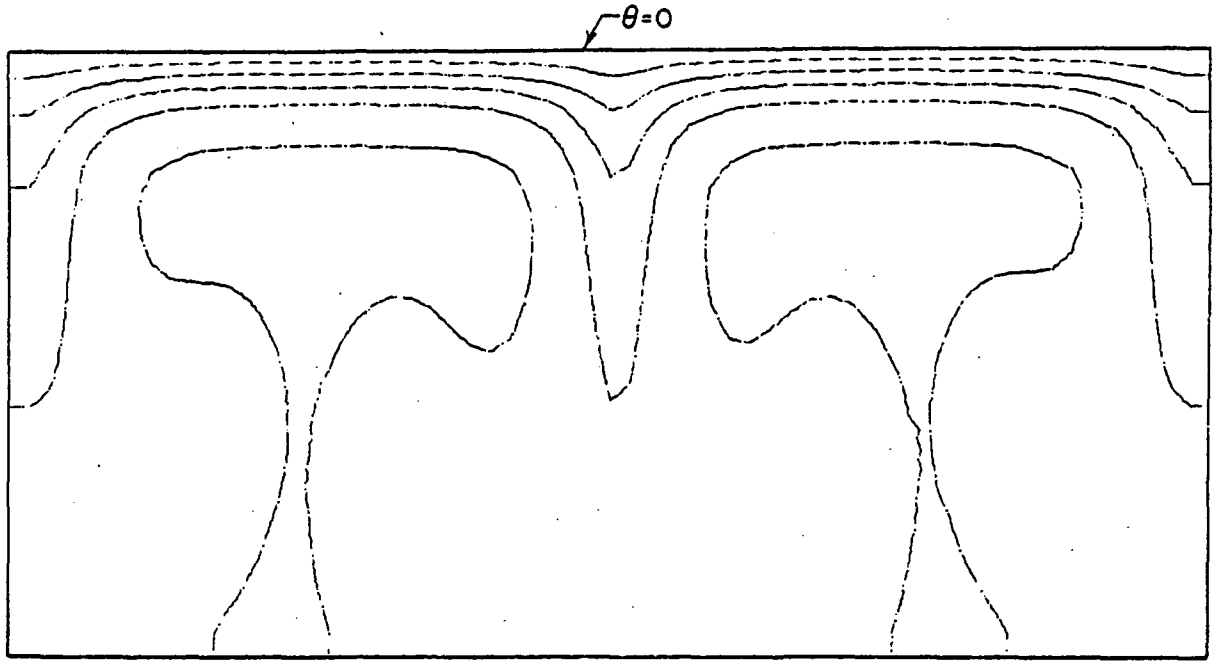

Fig. 12 - Isotherm pattern. Ra = 5 x 10^5, Pr = 6.5, and $\Delta\theta$ = 0.04

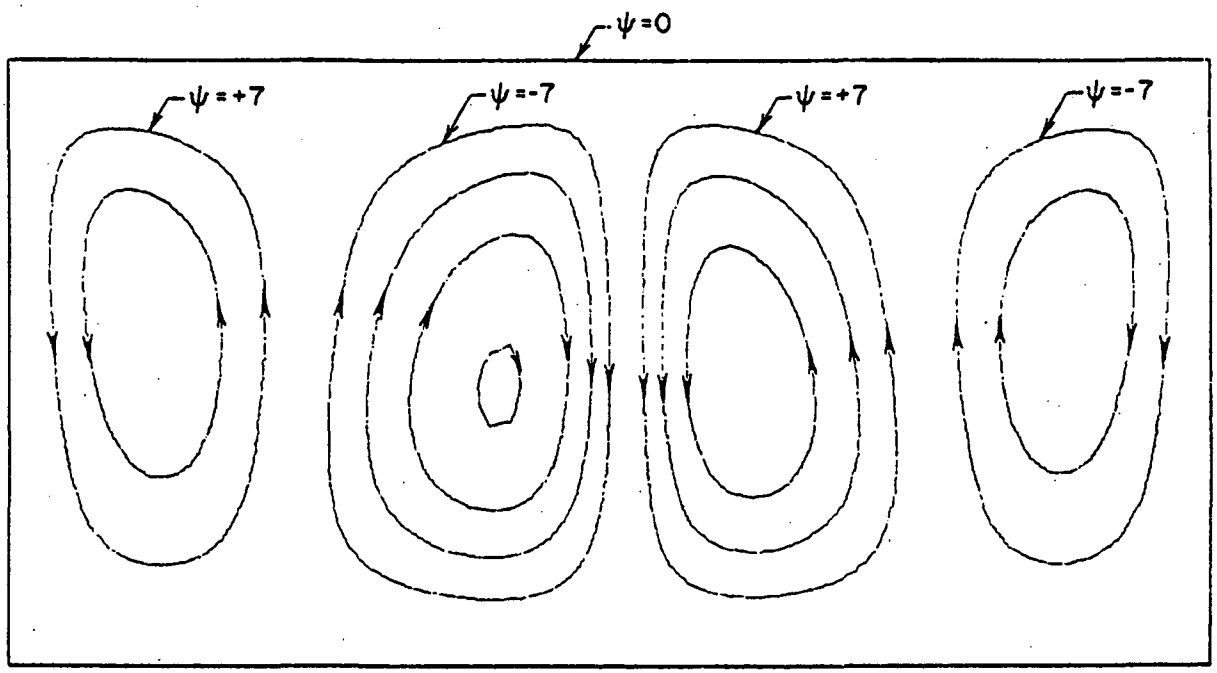

Fig. 13 - Streamline pattern. Ra = 10^6 and Pr = 6.5

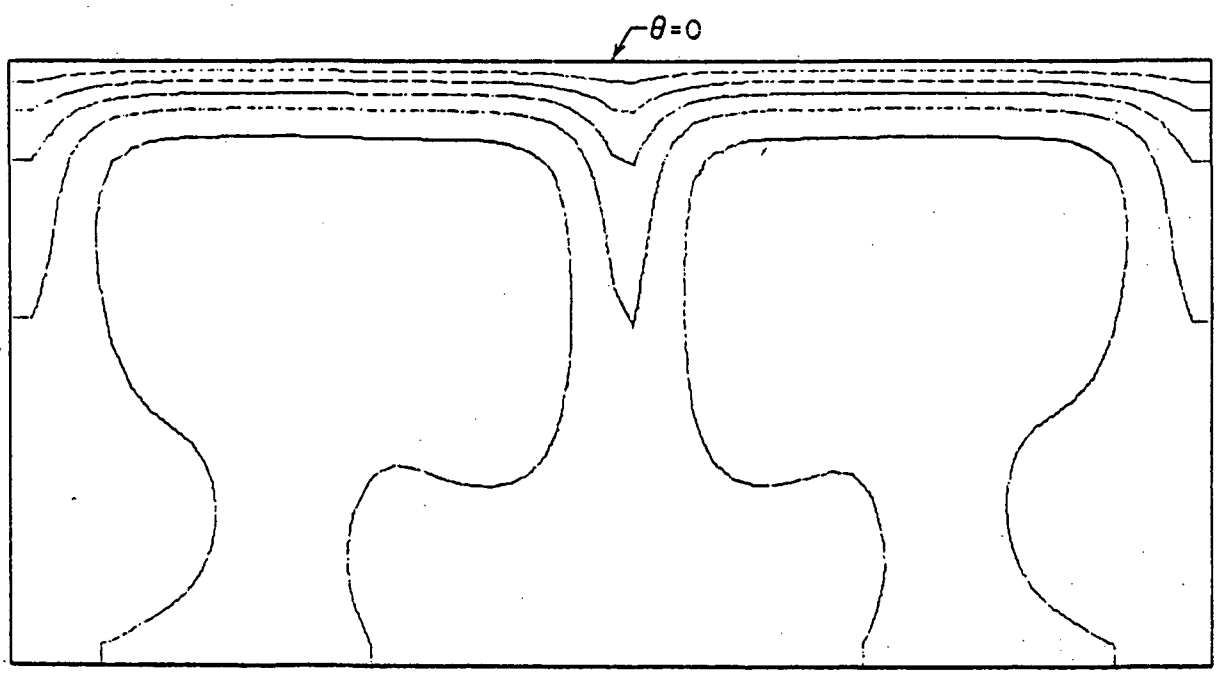

Fig. 14 - Isotherm pattern. Ra = 10^6, Pr = 6.5, and $\Delta\theta$ = 0.035

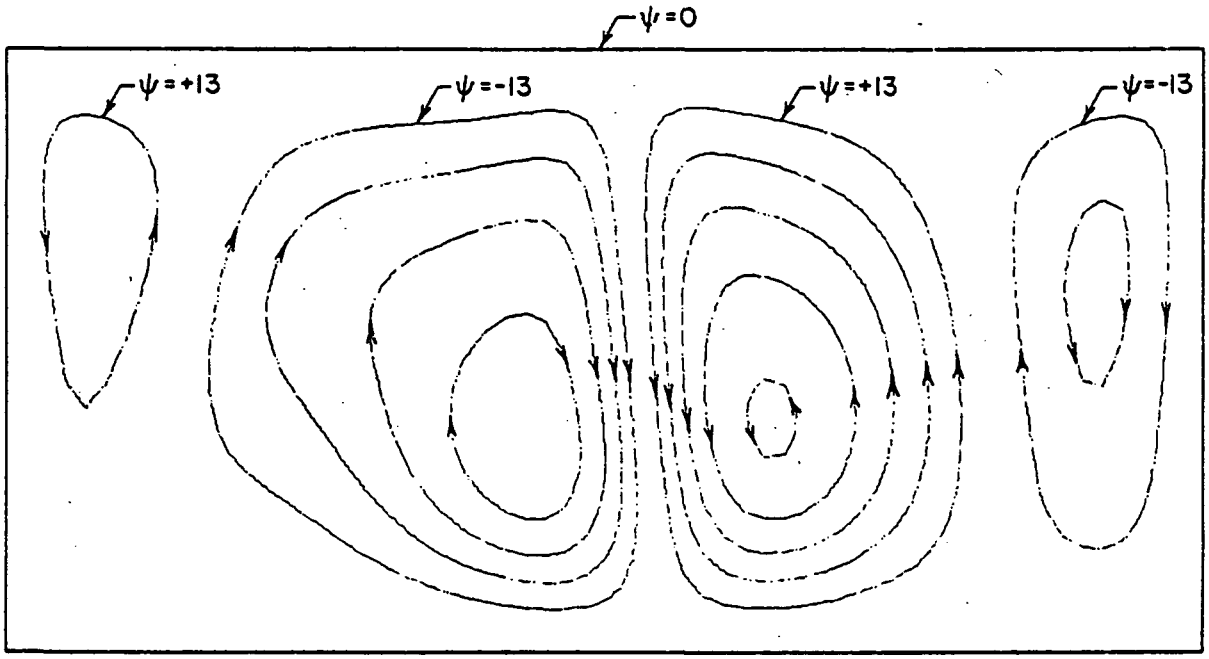

Fig. 15 - Streamline pattern. Ra = 5 x 10^6 and Pr = 6.5

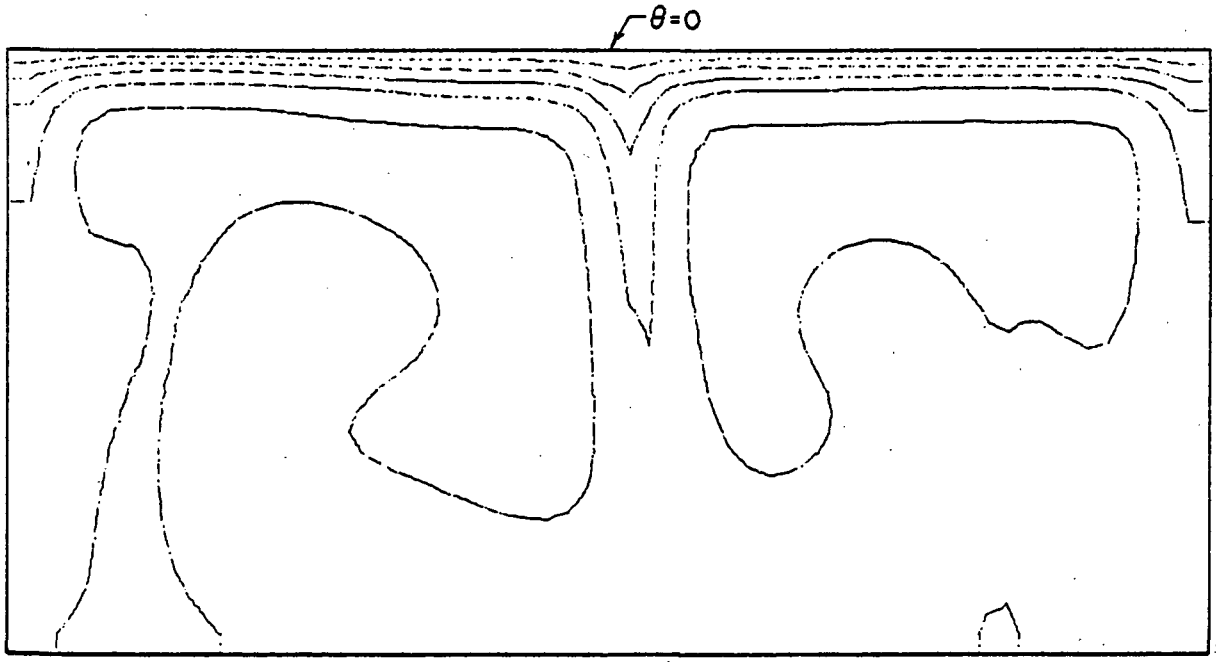

Fig. 16 - Isotherm pattern. Ra = 5 x 10^6, Pr = 6.5, and $\Delta\theta$ = 0.028

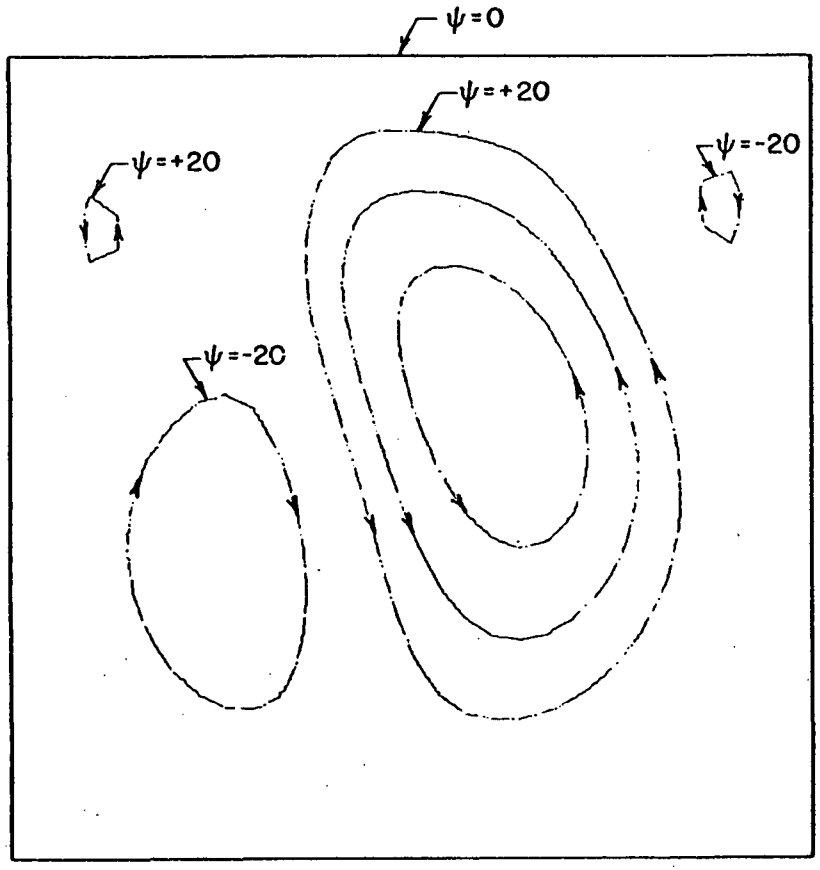

Fig. 17 - Streamline pattern. $Ra = 10^7$ and $Pr = 6.5$

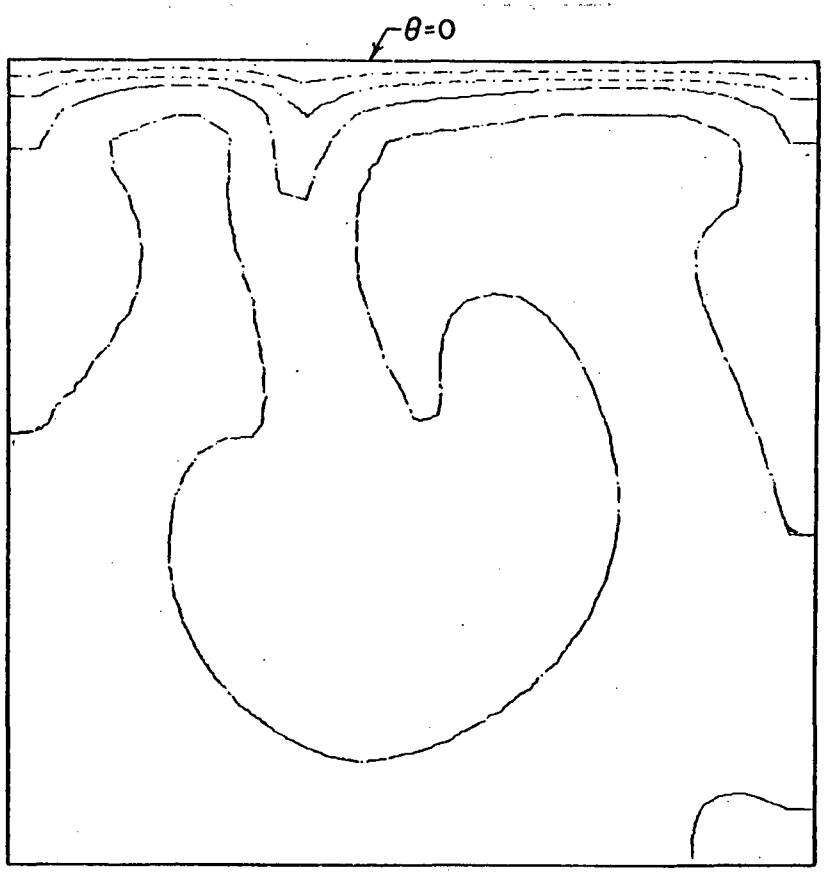

Fig. 18 - Isotherm pattern. $Ra = 10^7$, $Pr = 6.5$, and $\Delta\theta = 0.03$

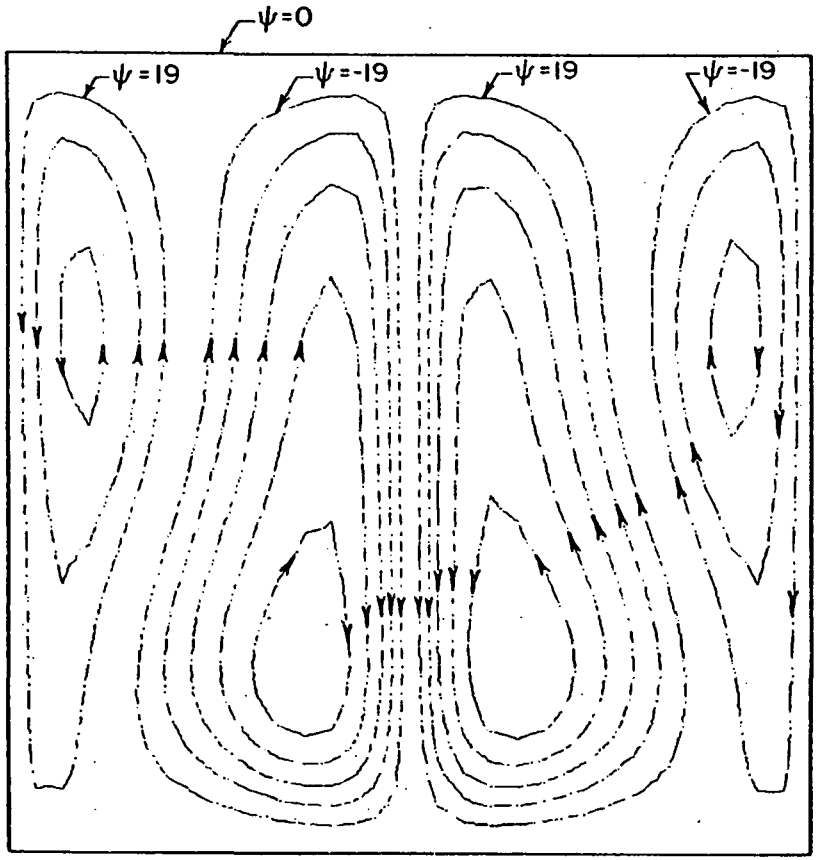

Fig. 19 - Streamline pattern. Ra = 10^8 and Pr = 6.5

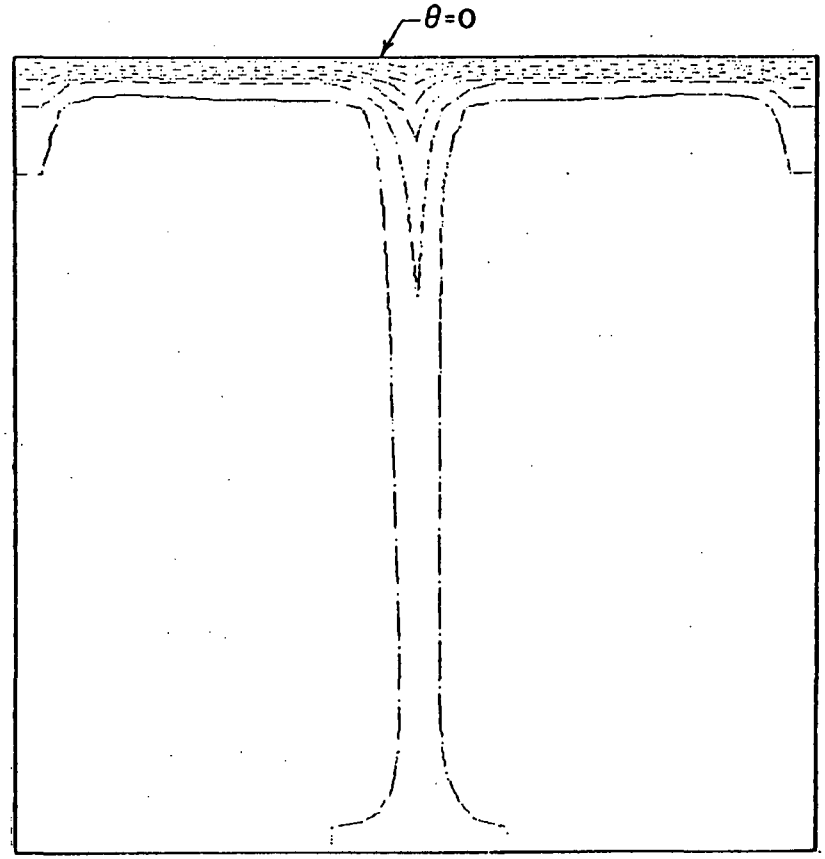

Fig. 20 - Isotherm pattern. Ra = 10^8, Pr = 6.5, and $\Delta\theta$ = 0.009

occupy about equal fractions the horizontal extent of the layer. These flow and temperature fields do not persist, however, as the Rayleigh number is increased to a value of 10^5 ($Ra/Ra_c = 72$). At this Rayleigh number, the flow field is characterized by a reversal in the direction of flow at the center of the layer (Fig. 10) and the formation of four counter-rotating swirls (Fig. 9). The regions of down-flow and up-flow still occupy about equal fractions of the horizontal extent of the layer, and the up-flow is a relatively broad region corresponding to each pair of swirls. The region of down-flow, however, becomes thiner at a Rayleigh number of 5×10^5 ($Ra/Ra_c \simeq 360$) as shown in Figs. 11 and 12. At $Ra = 10^6$ ($Ra/Ra_c \simeq 722$), the flow is still driven by four counter-rotating swirls (Fig. 13), and the broad region of warm up-flow (Fig. 14) has a horizontal extent somewhat larger than $Ra = 5 \times 10^5$. In Figs. 15-18, the existence of large-scale eddy motion becomes evident. The streamline patterns for $Ra = 5 \times 10^6$ and 10^7 have lost some of the regularity observed in the streamline patterns at lower Rayleigh numbers. Isotherm patterns at these same Rayleigh numbers show that thermals released from the thermal boundary layer at the upper surface have a scale of the order of the layer depth. For both of these Rayleigh numbers, down-flows occur in relatively narrow regions except when a thermal is released from the upper surface (Fig. 18), and up-flows occupy more of the horizontal extent of the layer. Thus, at these Rayleigh numbers, down-flows are considerably higher in velocity than the up-flow. At a Rayleigh number of 10^8 (Figs. 19 and 20), these features are even more pronounced.

In Figs. 21-28, isotherms and streamlines for $Pr = 1$ at different Rayleigh numbers are presented. The isotherms and streamlines presented in Figs. 21-24 at $Ra = 10^5$ and 5×10^5 show a form similar to those presented in Figs. 9-12 at $Pr = 6.5$ and the same Rayleigh numbers. At these low Rayleigh numbers, the gross features of the flow and temperature fields are apparently independent of the Prandtl number. Comparing the streamlines and isotherms for a Rayleigh number of 10^6 and $Pr = 1$ (Figs. 24 and 25) with those obtained with $Pr = 6.5$ and at the same Rayleigh number (Figs. 13 and 14), one can see that although four swirls exist in both cases, a slight difference appears in the features of the isotherms. In Figs. 26 and 27 are shown the streamlines and isotherms for a Rayleigh number of 5×10^6. These isotherms and the streamlines can be best compared with those presented in Figs. 15 and 16 for $Pr = 6.5$. While at a Prandtl number of 6.5, three tongues of down-flow exist in the layer; at $Pr = 1$ only two such tongues appear. At the larger Prandtl number, the convective motion splits into more swirls than at lower Prandtl numbers.

To gain further insight on the influence of the Prandtl number, Figs. 29 and 30 contain the results for $Pr = 0.05$ and $Ra = 5 \times 10^6$, and Figs. 30 and 31 contain the results for the same Rayleigh number but for $Pr = 20$. A Rayleigh number of 5×10^6 has been chosen because at this value the difference between the convection form for $Pr = 6.5$ and $Pr = 1$ is significant. At $Pr = 0.05$, the isotherm pattern (Fig. 30) indicates that conduction is a dominant mechanism for energy transport near the upper boundary, more so than at higher Prandtl numbers (compare Fig. 30 with Fig. 32). At the lower Prandtl numbers, the flow is characterized

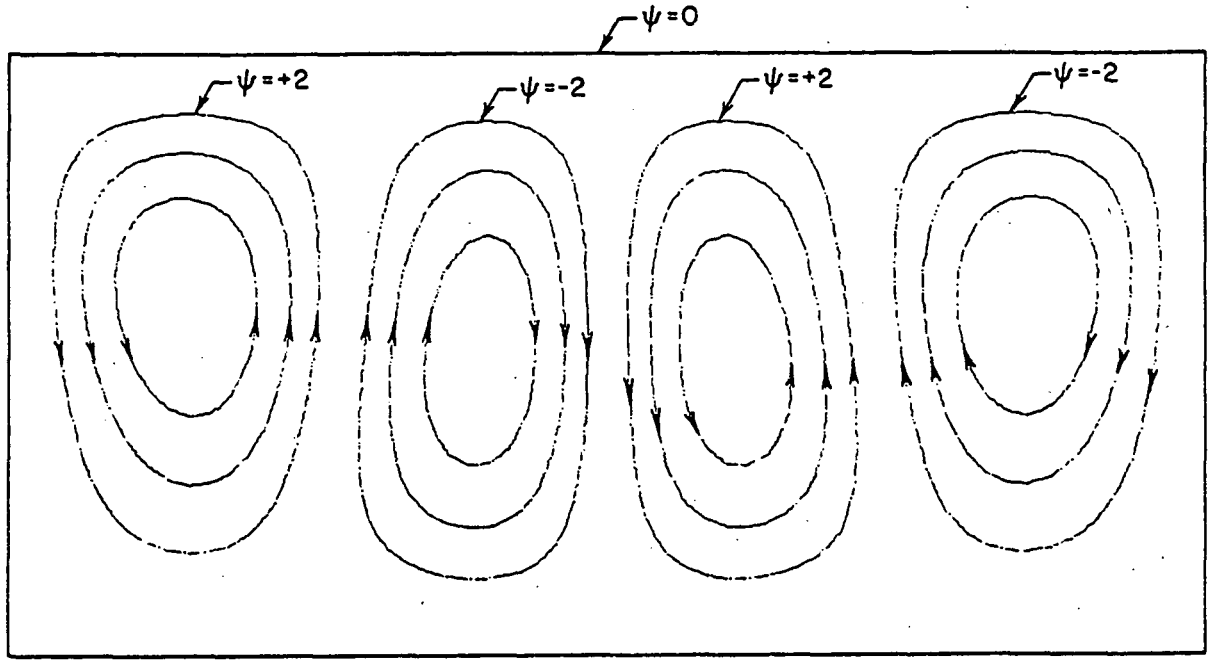

Fig. 21 - Streamline pattern. | Ra = 10^5 and Pr = 1

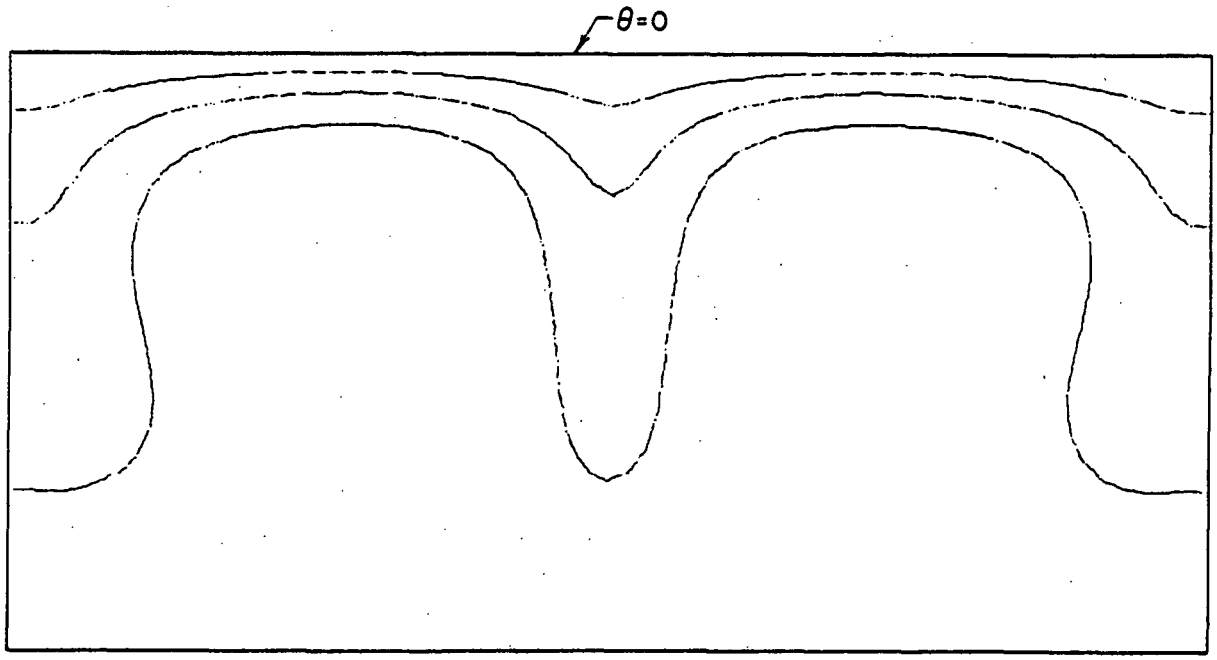

Fig. 22 - Isotherm pattern. | Ra = 10^5, Pr = 1, and $\Delta\theta$ = 0.077

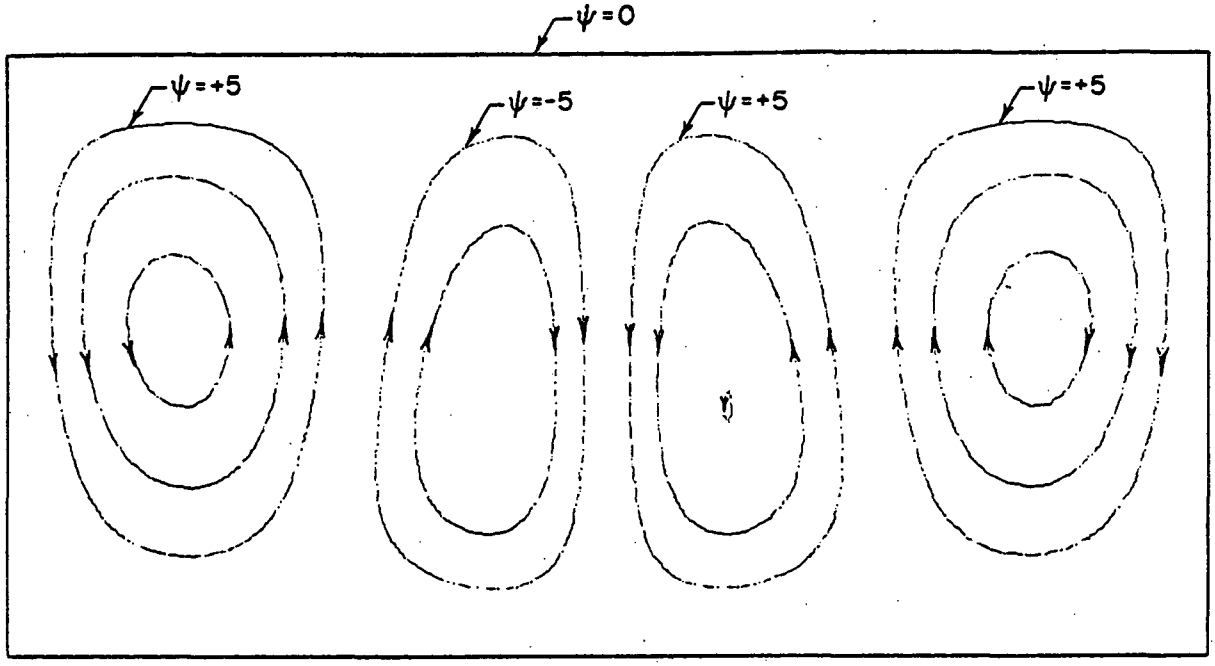

Fig. 23 - Streamline pattern. Ra = 5 x 10^5 and Pr = 1

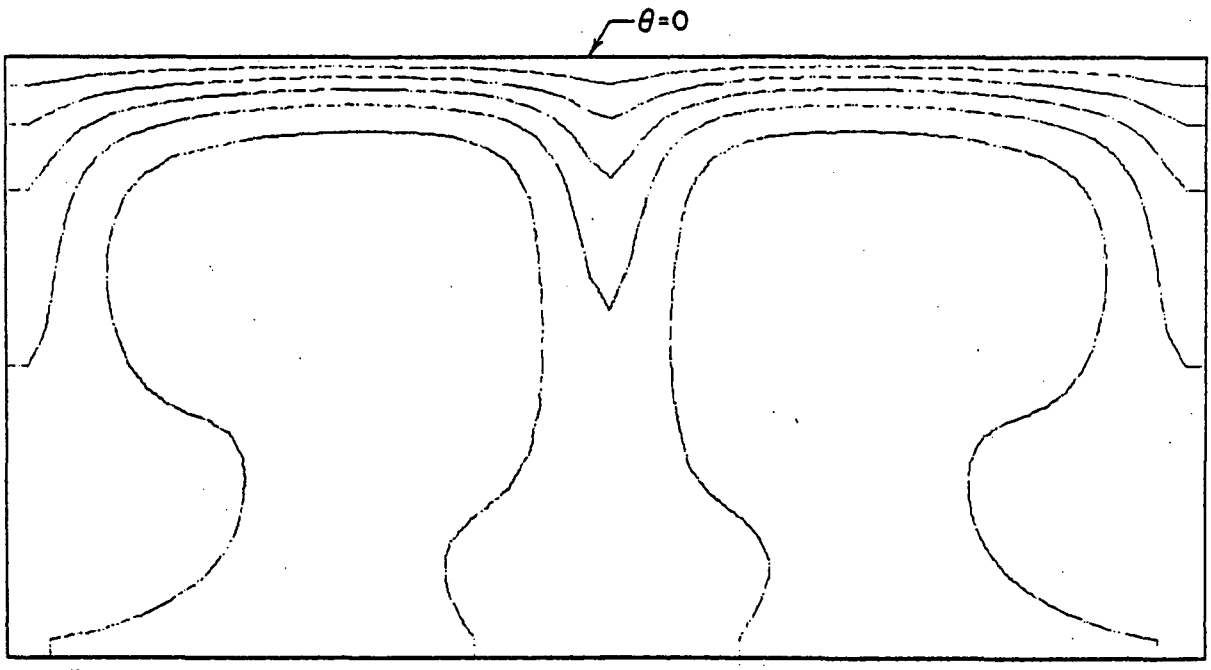

Fig. 24 - Isotherm pattern. Ra = 5 x 10^5, Pr = 1, and $\Delta\theta$ = 0.04

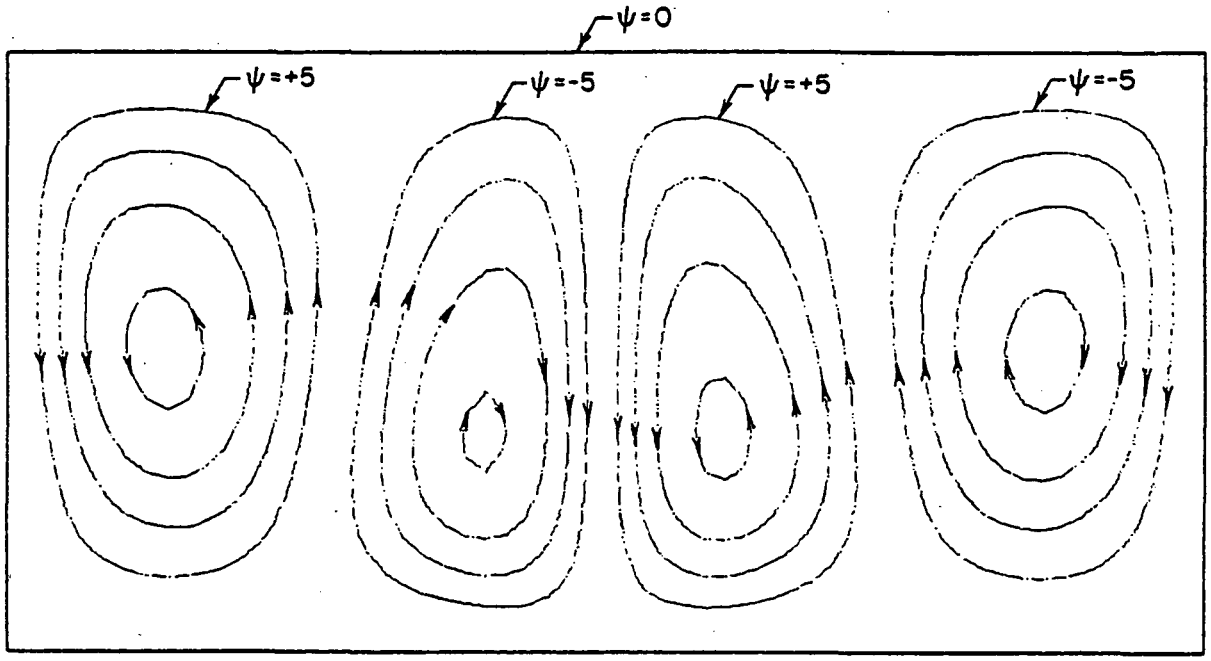

Fig. 25 - Streamline pattern. | Ra = 10^6 and Pr = 1

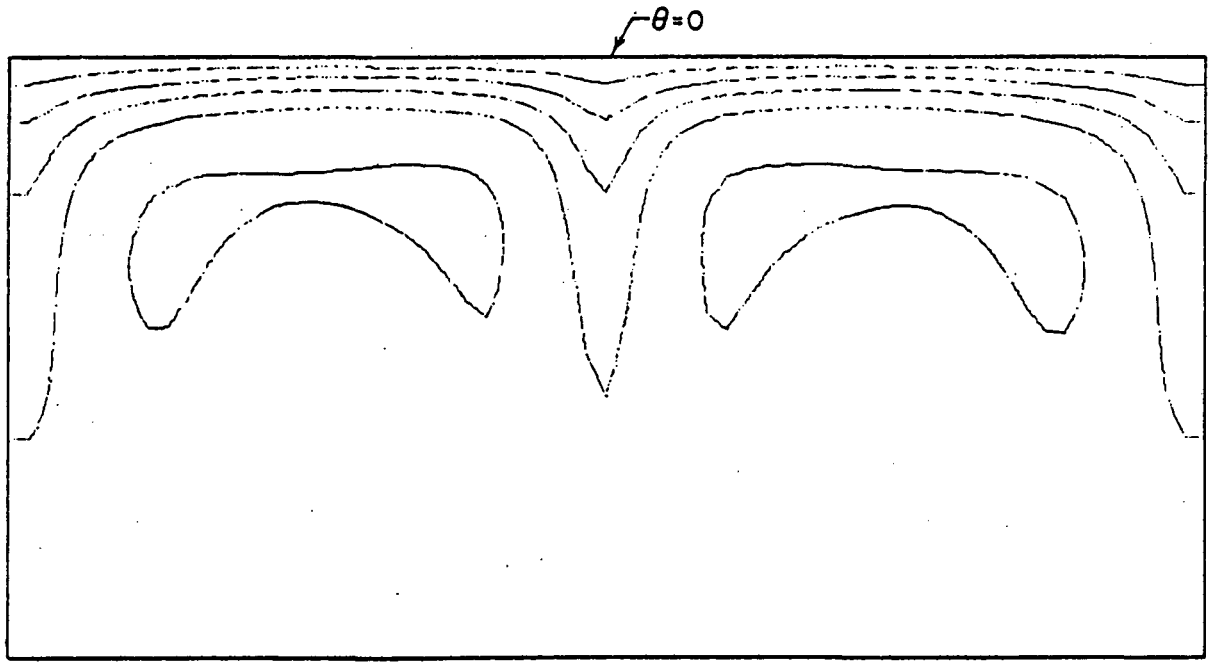

Fig. 26 - Isotherm pattern. | Ra = 10^6, Pr = 1, and $\Delta\theta$ = 0.04

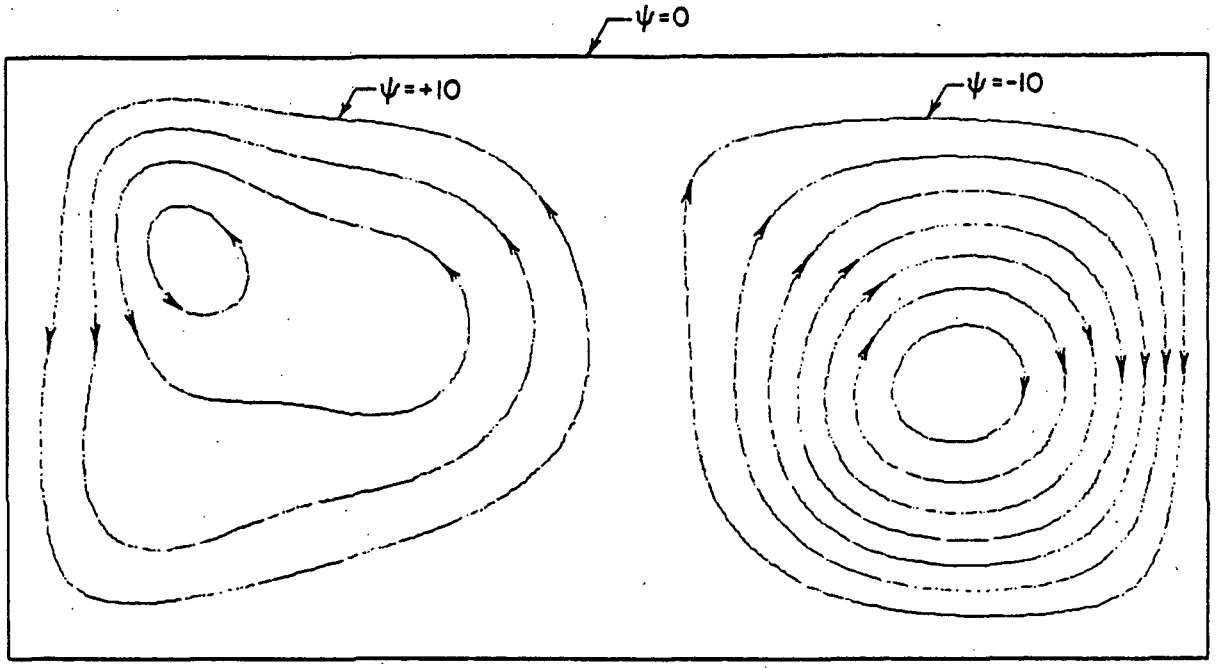

Fig. 27 - Streamline pattern. Ra = 5 x 10^6 and Pr = 1

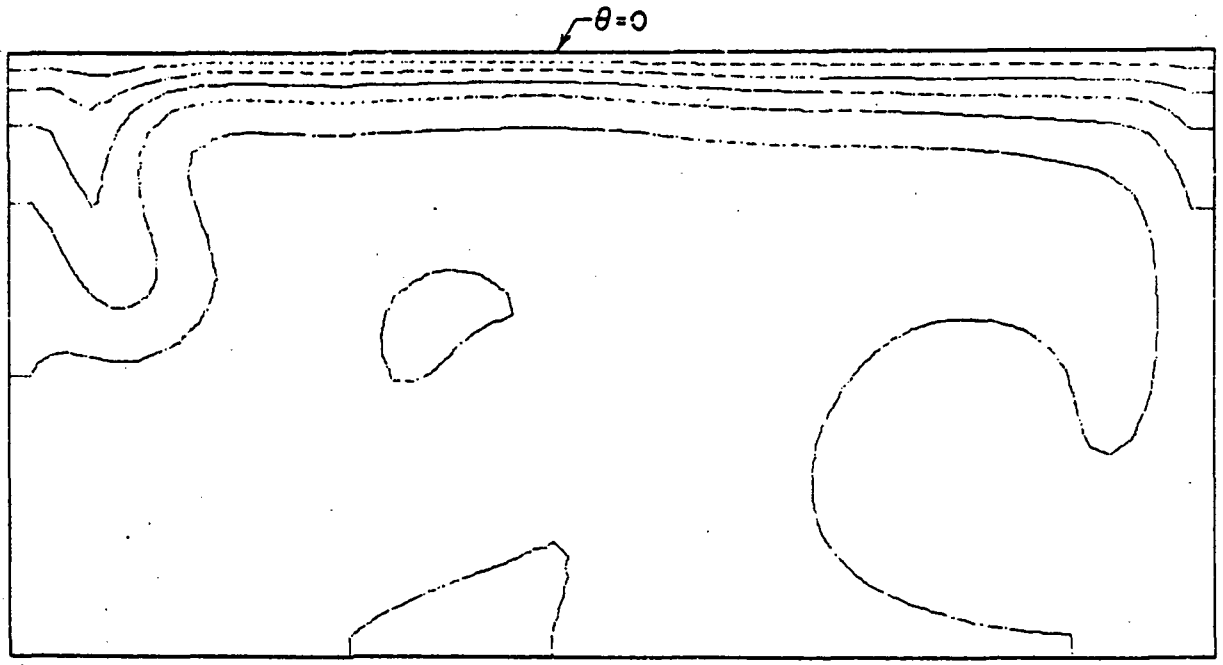

Fig. 28 - Isotherm pattern. Ra = 5 x 10^6, Pr = 1, and $\Delta\theta$ = 0.035

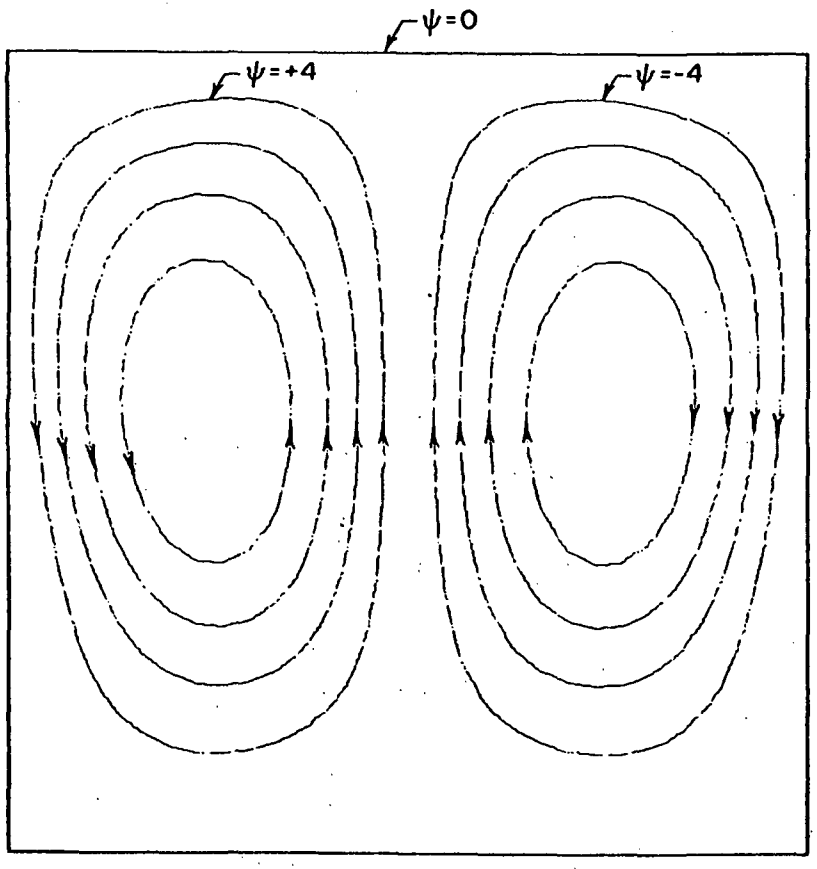

Fig. 29 - Streamline pattern. $Ra = 5 \times 10^6$ and $Pr = 0.05$

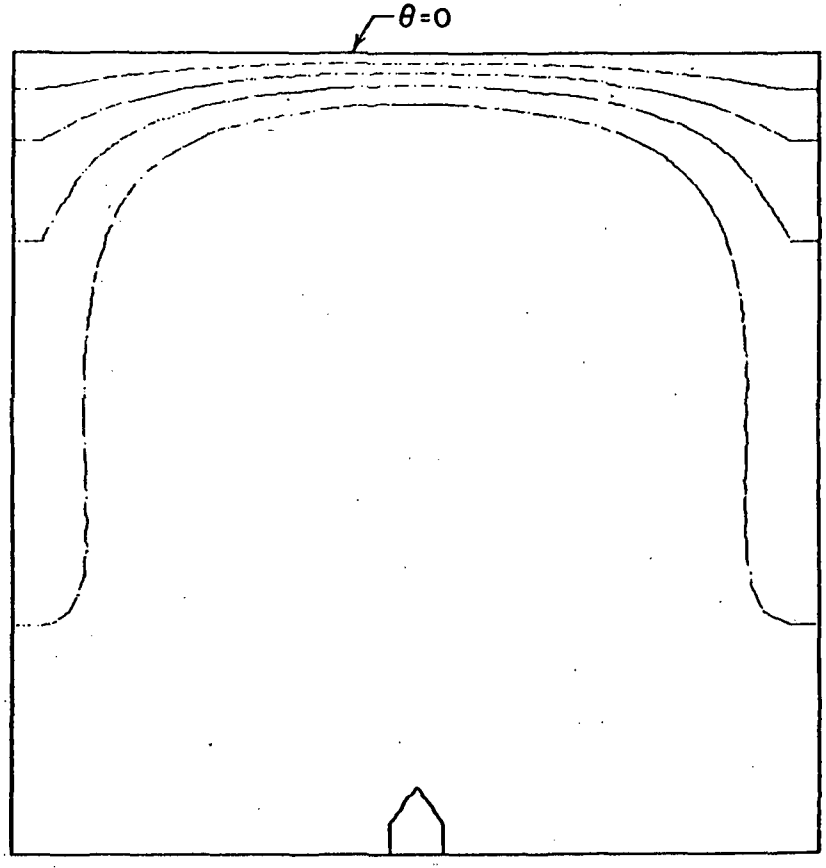

Fig. 30 - Isotherm pattern. $Ra = 5 \times 10^6$, $Pr = 0.05$, and $\Delta\theta = 0.038$

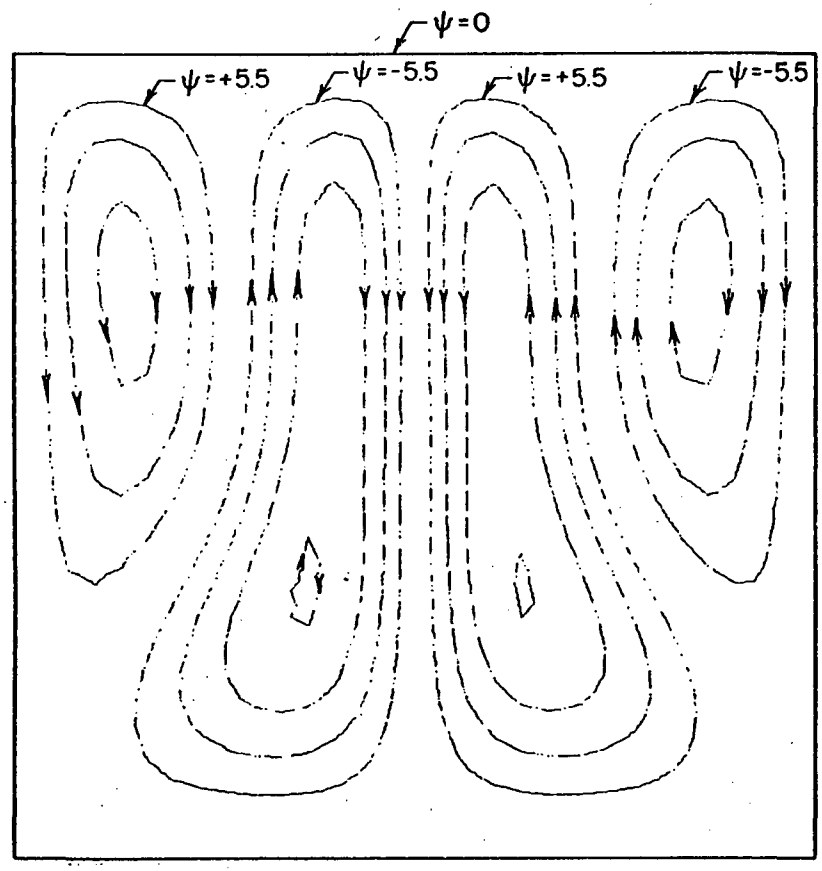

Fig. 31 - Streamline pattern. $Ra = 5 \times 10^6$ and $Pr = 20$

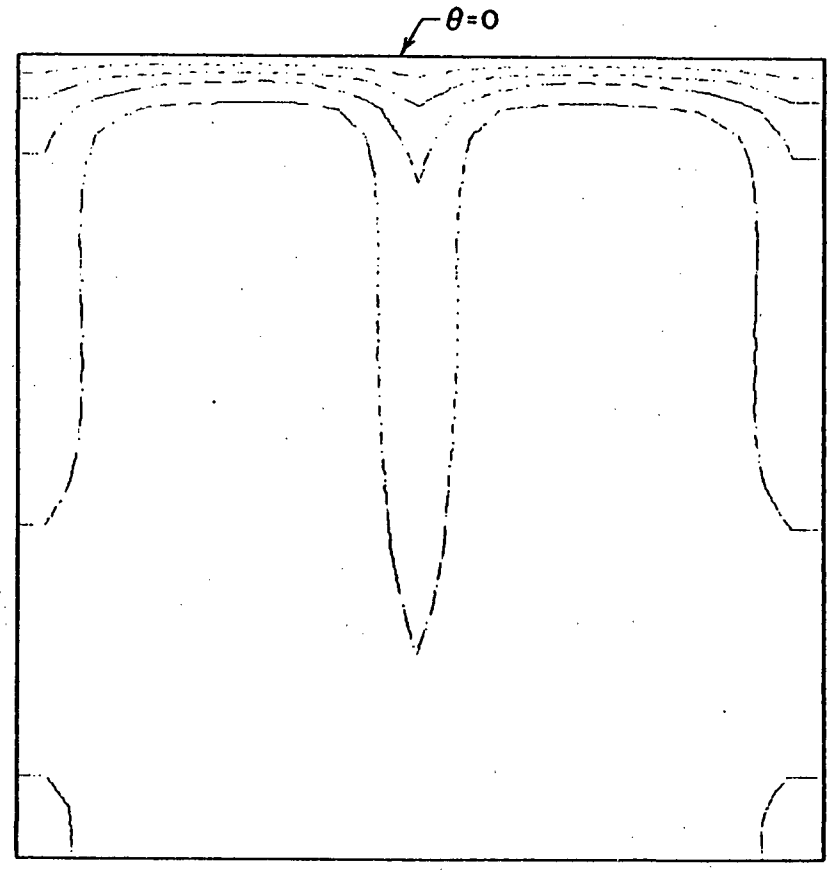

Fig. 32 - Isotherm pattern. $Ra = 5 \times 10^6$, $Pr = 20$, and $\Delta\theta = 0.025$

by the absence of narrow regions of down-flow from the upper surface and fewer regions (swirls) of circulating flow (compare Fig. 29 with Fig. 31). A comparison of Fig. 30 with Fig. 32 reveals that the thermal boundary layer at the upper surface is much thicker at the lower Prandtl number. A comparison of Fig. 29 with Fig. 31 shows, also, that at Pr = 0.05 the distance between streamlines in the down-flow zones is about the same in the regions of up-flow. This means that in both regions, the velocities are about the same. On the other hand, at Pr = 20 it is clear that the velocity in the down-flow region is much higher than in the region of up-flow.

The temperature fields for steady convection enable one to calculate the average heat flux at the upper boundary and the horizontally averaged temperature distribution in the layer. From these quantities, it is possible to determine the overall Nusselt number at the upper boundary. It was found that the Nusselt number and Rayleigh number could be correlated by

$$\left.\begin{aligned} &Nu_1 = 0.420\ Ra^{0.223} \\ &5 \times 10^3 \leq Ra \leq 5 \times 10^8 \\ &Pr = 6.5,\quad 0.125 \leq L/X \leq 1 \end{aligned}\right\}, \tag{60}$$

and

$$\left.\begin{aligned} &Nu_1 = 0.477\ Ra^{0.210} Pr^{0.0407} \\ &5 \times 10^3 \leq Ra \leq 5 \times 10^8 \\ &0.05 \leq Pr \leq 20 \\ &0.125 \leq L/X \leq 1 \end{aligned}\right\}. \tag{61}$$

Agreement between the correlation obtained numerically, Eq. (60), and that obtained experimentally by Kulacki and Emara [8] is very good (Fig. 33). The numerically derived correlation differs by less than 2% from the experimental results for low Rayleigh numbers (i.e., $10 \leq Ra/Ra_c \leq 38$) and both correlations are nearly identical at higher Rayleigh numbers. A comparison between the numerical results for the heat transfer coefficient of this study, Eq. (60), and numerical work of Thirlby [16] using the method of artificial compressibility and Roberts' analytical results [15] are presented in Fig. 34 along with the experimental data of Kulacki and Emara [8]. It can be seen in Fig. 34 that the results of the present study give better agreement with the experimental data of Kulacki and Emara than either of the other studies.

Horizontally averaged temperature distributions across the layer obtained numerically in this study are compared with the measurements of

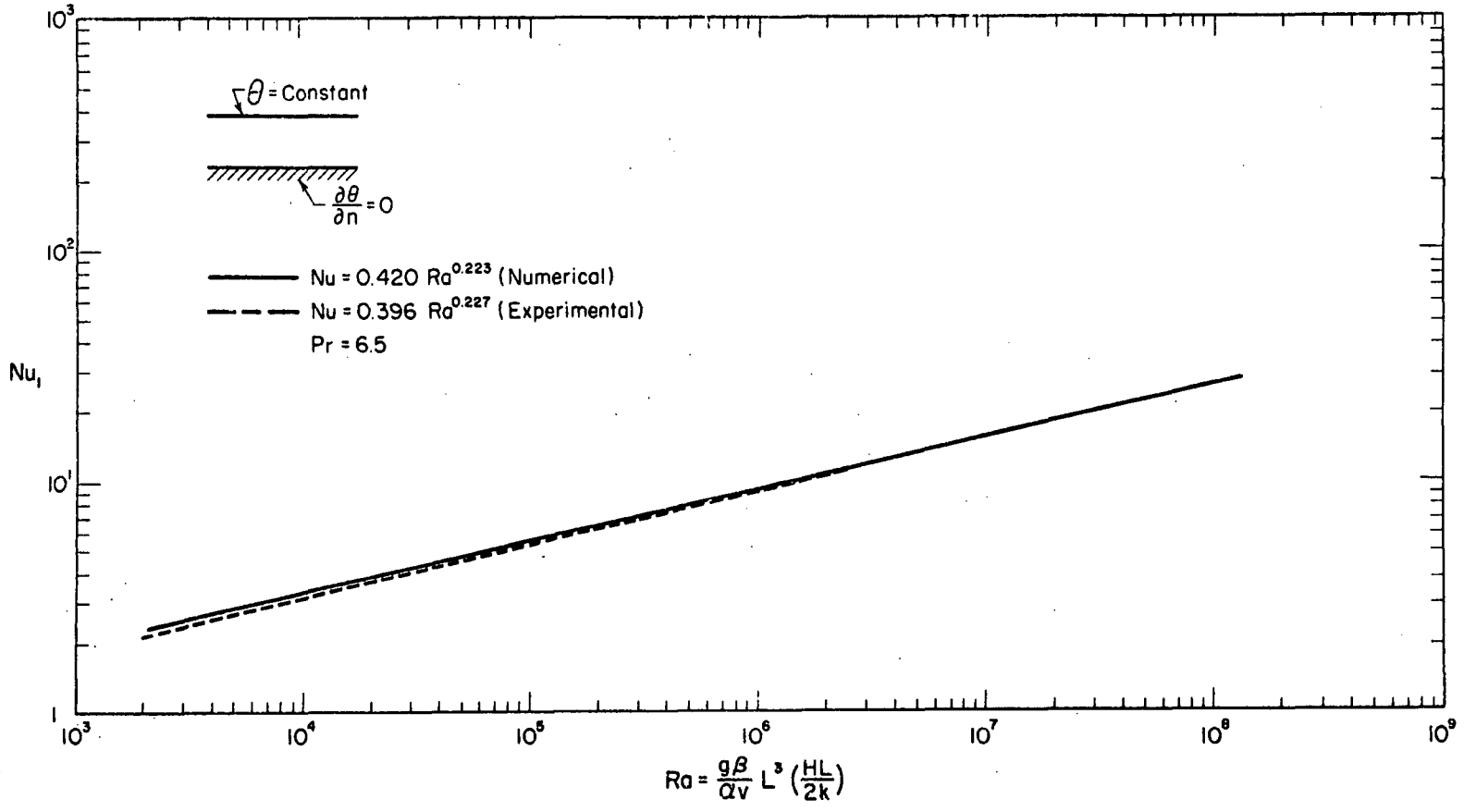

Fig. 33 - Heat transfer correlation of the present study and that of Kulacki and Emara [8] for a layer with a rigid, isothermal upper boundary and a rigid, zero heat flux lower boundary

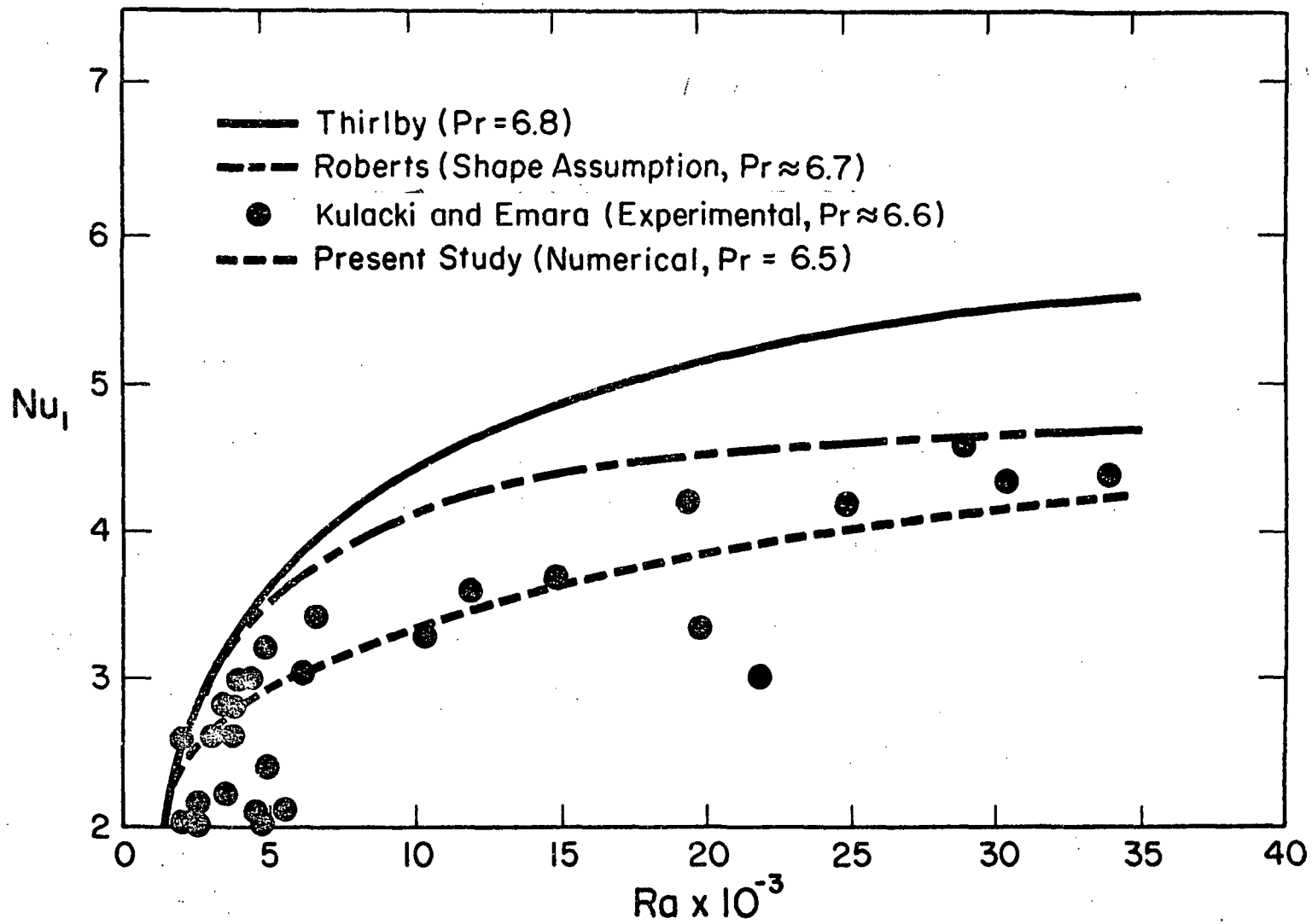

Fig. 34 - Nusselt numbers at the upper boundary from the present study and the studies of Roberts [15], Thirlby [16], and Kulacki and Emara [9]

Kulacki and Emara [9] in Figs. 35-37. Good agreement is seen between the numerical and experimental results. The deviation between the experimental and numerical temperature profiles in the core region (Figs. 36 and 37) is believed to be caused by the disturbances of the flow introduced by a thermocouple probe which was used to obtain time-averaged measurements of temperature within the layer. Numerical results for the horizontally averaged maximum temperature difference across the layer are compared in Fig. 38 with the experimental results of Kulacki and Emara. The agreement between the measured and computed values is seen to be good over the range of Rayleigh numbers considered in the present study.

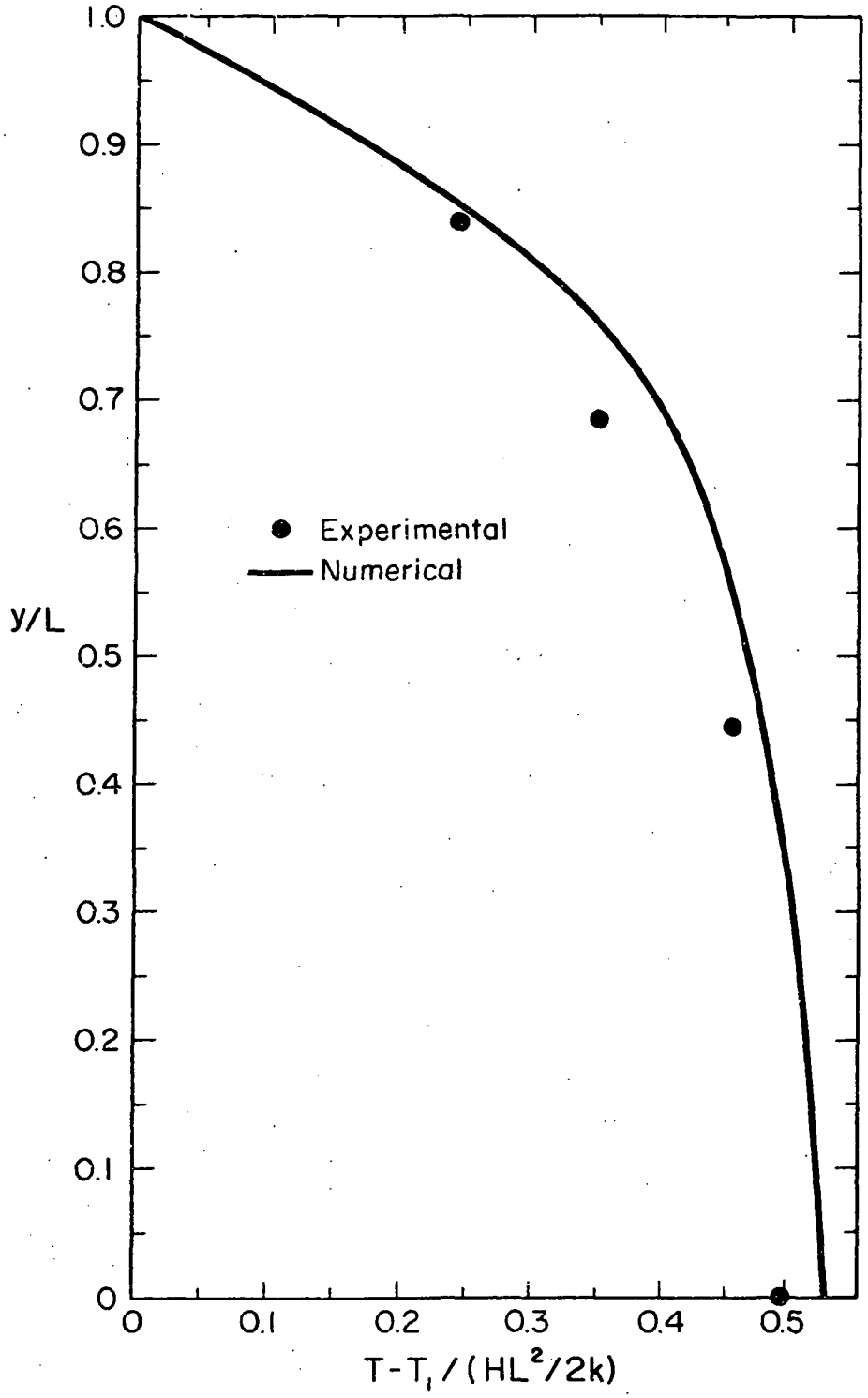

Fig. 35 - Horizontally averaged temperature distribution determined numerically and the time averaged measurements of Kulacki and Emara [9] for Ra = 5.59×10^4

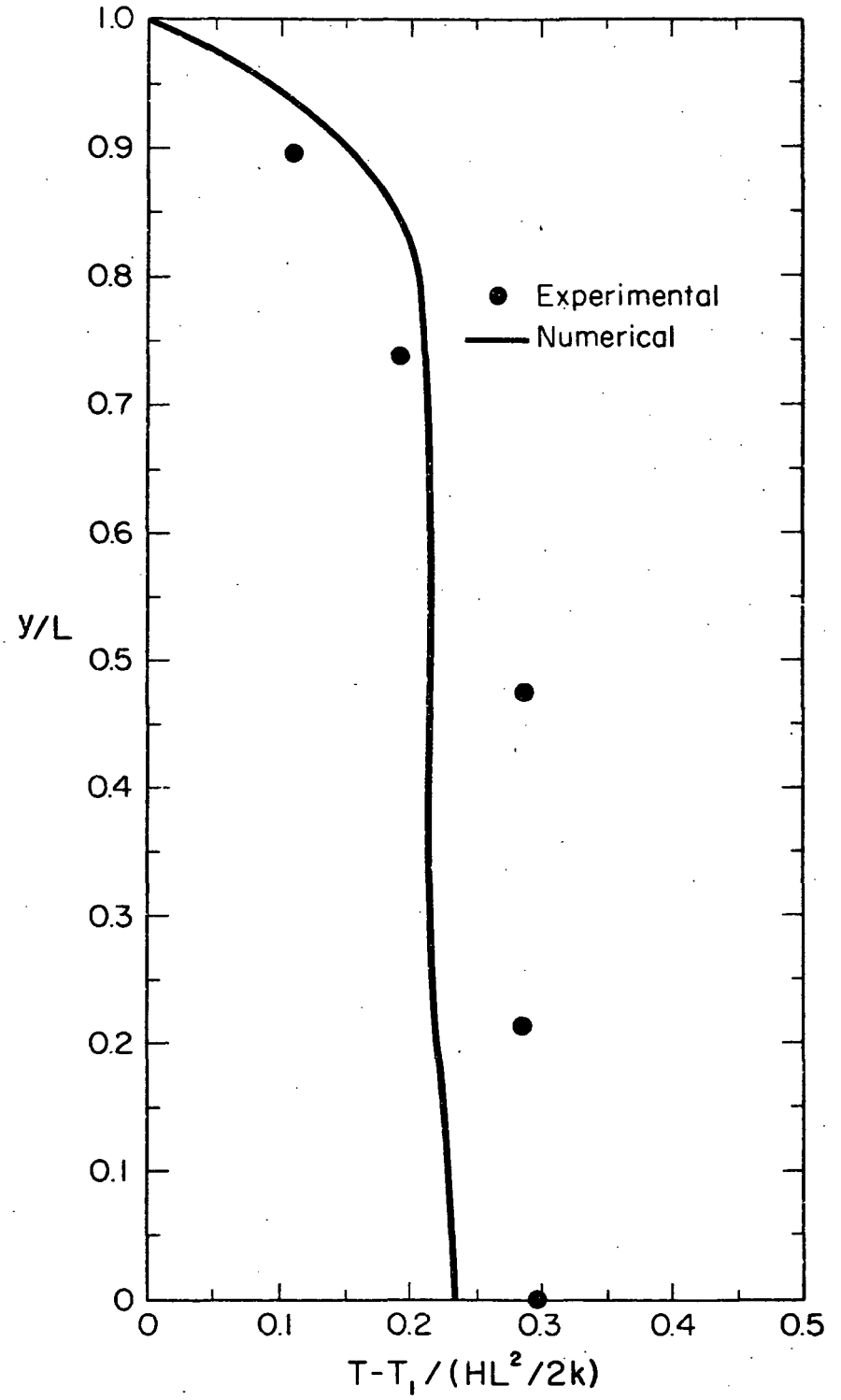

Fig. 36 - Horizontally averaged temperature distribution determined numerically and the time averaged measurements of Kulacki and Emara [9] for Ra = 2.85×10^5

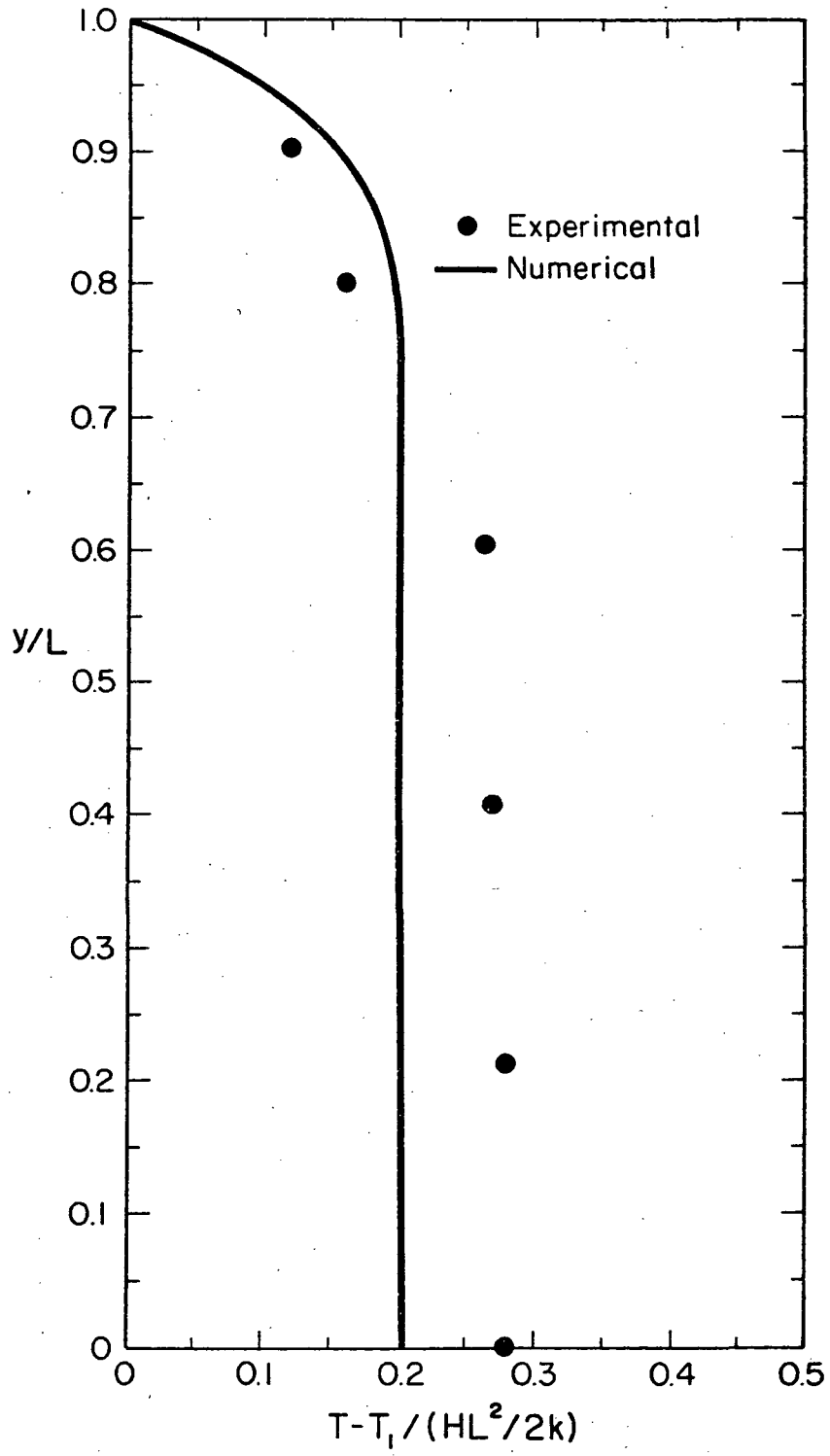

Fig. 37 - Horizontally averaged temperature distribution determined numerically and the time averaged measurements of Kulacki and Emara [9] for Ra = 8.55×10^5

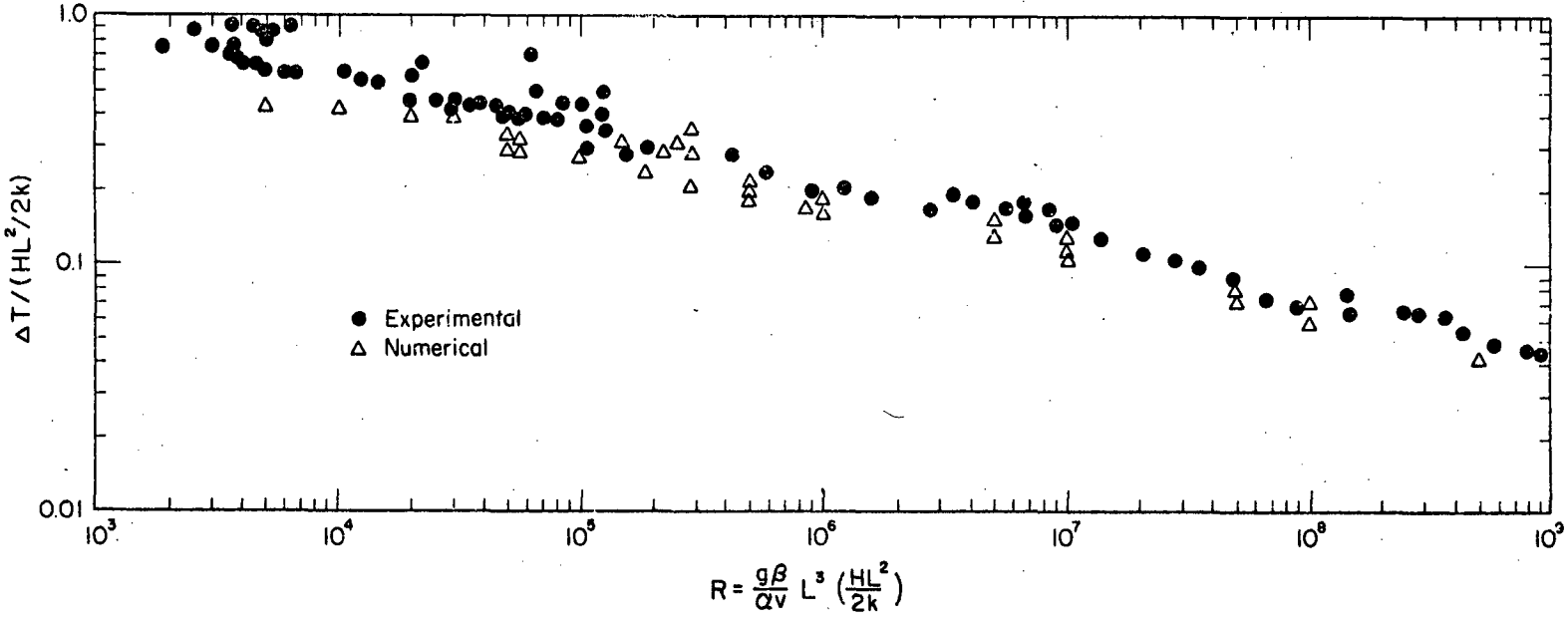

Fig. 38 - Horizontally averaged maximum temperature difference across the layer and the measurements of Kulacki and Emara [8]

SECTION V - CONCLUDING REMARKS

The present study has resulted in a numerical solution of the partial differential equations which govern thermal convection with uniform volumetric energy sources in a horizontal fluid layer. The boundary conditions of primary concern are a rigid, isothermal upper boundary and a rigid, zero-heat-flux lower boundary. The side walls are assumed to be rigid and perfectly insulating. Subsidiary calculations have been done for a fluid layer with two rigid, isothermal horizontal boundaries with both side walls rigid and perfectly insulating. These calculations serve as a check on the numerical formulation of the problem owing to the existence of both experimental and numerical studies for a layer with these boundary conditions.

The numerical results for the temperature distribution within the layer permit the computation of the average heat transfer coefficient at the upper boundary. A correlation of the Nusselt number in terms of the Rayleigh and Prandtl numbers has been determined in the following form:

$$Nu_L = 0.477\ Ra^{0.210} Pr^{0.0407}$$

$$5 \times 10^3 \leq Ra \leq 5 \times 10^8$$

$$0.05 \leq Pr \leq 20$$

$$0.125 \leq L/X \leq 1 \ .$$

When this form of correlation is restricted to the results for Pr = 6.5, predicted Nusselt numbers are in excellent agreement with the measurements of Kulacki and Emara [8]. The results of the present study are thus confirmed by the experiments for $Ra \leq 5 \times 10^8$ [Eq. (60) and Fig. 33].

The results of the present study are formally restricted to two-dimensional laminar convection. While the horizontally averaged temperature profiles and the correlation for the Nusselt number derived from them are in agreement with the measurements of Kulacki and Emara [8,9], it should be noted that the Rayleigh number range considered overlaps what is believed to be the turbulent regime of flow. The early experiments of Tritton and Zarraga [18] on the planform of the motion in a layer with boundary conditions similar to those of the present study showed that turbulent motion begins at a Rayleigh number on the order of 80 times the critical value for the onset of convection predicted by linear stability theory. More recent experiments by Kulacki and Goldstein [7] on a layer with two isothermal boundaries indicated that turbulent motion begins at Rayleigh numbers about 100 times the critical value. The work of Tritton and Zarraga, however, is considered as the only substantiated indication of the onset of turbulence in the system of interest here. The critical Rayleigh number given by linear stability theory is $Ra_c = 1386$ [10], and this places the results of the present study in the range $3.61 \leq Ra/Ra_c \leq 3.6 \times 10^5$. Thus the general validity of the isotherm and streamline

patterns for high Rayleigh numbers of the present study can be questioned despite the agreement between computed and measured Nusselt numbers. It is, indeed, possible that overall heat transfer results are relatively insensitive to the details of the flow field within the layer as long as the scale of the motion (e.g., see Figs. 15-20) is of the order of the layer depth. A recent study by Cheung [3], who developed a semiempirical model for turbulent convection, supports this contention. On the other hand, numerically induced viscosity effects may essentially inhibit the destabilizing effects of turbulence in the finite-difference computations. These and other issues related to the validity of finite-difference calculations of thermal convection over a wide range of Rayleigh numbers can be resolved only after further analytical and numerical investigation.

In its present form, the computer program developed in this study will enable computations of thermal convection to be carried out for a variety of thermal and hydrodynamic boundary conditions of interest to both fluid dynamicists and engineers. For example, it is of interest to determine the influence of a free upper surface on the heat transfer coefficient at the upper boundary and on the overall flow field within the layer. Additional computations on the effect of conducting side walls or, equivalently, horizontal mean temperature gradients greater than zero on the heat transfer rate to the upper boundary would be of interest in the fields of geophysics and nuclear safety engineering. These calculations are presently being carried out, and the results will be forthcoming.

REFERENCES

1. Barakat, H. Z., and Clark, J. A., "Analytical and Experimental Study of Transient Laminar Natural Convection Flow in Partially Filled Liquid Containers," Proceedings, Third International Heat Transfer Conference, Chicago, Illinois (1966).

2. Chandrashekhar, S., Hydrodynamic and Hydromagnetic Stability, Oxford, London (1961).

3. Cheung, F. B., "Natural Convection in a Volumetrically Heated Fluid Layer at High Rayleigh Numbers," International Journal Heat and Mass Transfer, Vol. 20 (1977), pp. 499-506.

4. Emara, A. A., On Natural Convection with Internal Heating in Fluid Layers, Ph.D. Dissertation in Mechanical Engineering, The Ohio State University (1977).

5. Fromm, J., "The Time Dependent Flow of an Incompressible Viscous Fluid," Methods in Computational Physics, Vol. 3, Academic Press, New York, p. 345.

6. Goldstein, R. J.; Chu, T. Y.; and Kulacki, F. A., "Optical Studies of Thermal Convection," Engineering Societies Library, Heat Transfer Film Library, Catalog No. G-5, American Society of Mechanical Engineers, New York (1977).

7. Kulacki, F. A., and Goldstein, R. J., "Thermal Convection in a Horizontal Fluid Layer with Uniform Volumetric Energy Sources," Journal of Fluid Mechanics, Vol. 55 (1972), pp. 271-287.

8. Kulacki, F. A., and Emara, A. A., "High Rayleigh Number Convection in Enclosed Fluid Layers with Internal Heat Sources," U.S. Nuclear Regulatory Commission, NUREG-75-065 (July, 1975).

9. Kulacki, F. A., and Emara, A. A., "Transient Natural Convection in an Internally Heated Fluid Layer," U.S. Nuclear Regulatory Commission, Topical Report, NUREG-0078 (August, 1976).

10. Kulacki, F. A., and Goldstein, R. J., "Hydrodynamic Stability in Fluid Layers with Volumetric Energy Sources," Applied Scientific Research, Vol. 31 (1975), p. 81.

11. Lax, P. D., and Richtmeyer, R. D., "Survey of the Stability of Linear Finite-Difference Equations," Communications on Pure and Applied Mathematics, Vol. 9 (1956), p. 267.

12. Mayinger, F. X., Jahn, M., Reineke, H. H., and Steinberner, V., "Examination of Thermohydraulic Processes and Heat Transfer in a Core Melt," Federal Ministry for Research and Technology, Final

Report RS48/1, Vols. 1-5 (in German), Hannover, Federal Republic of Germany (July, 1975).

13. Mihaljan, J., "A Rigorous Exposition of the Boussinseq Approximation Applicable to a Thin Layer of Fluid," Astrophysical Journal, Vol. 136 (1962), p. 1126.

14. Roache, P. J., Computational Fluid Dynamics, Hermosa Publishers, Albuquerque (1972).

15. Roberts, P. H., "Convection in Horizontal Layers with Heat Generation, Theory," Journal of Fluid Mechanics, Vol. 30 (1967), pp. 33-41.

16. Thirlby, R., "Convection in an Internally Heated Fluid Layer," Journal of Fluid Mechanics, Vol. 44 (1970), pp. 673-693.

17. Torrance, K. E., "Comparison of Finite-Difference Computations of Natural Convection," Journal of Research of the National Bureau of Standards, Mathematical Sciences, Vol. 72B (1968), pp. 281-301.

18. Tritton, D. J., and Zarraga, M. N., "Convection in Horizontal Fluid Layers with Heat Generation, Experiments," Journal of Fluid Mechanics, Vol. 30 (1967), pp. 21-32.

19. Wilkes, J. O.; Carnahan, B.; and Luther, H. A., Applied Numerical Methods, John Wiley and Sons, New York (1969).